5-2021

A Study of Nanogenerator Based Flow Sensor

Farzana Tasnim
The University of Texas Rio Grande Valley

A STUDY OF NANOGENERATOR BASED FLOW SENSOR

A Thesis

by

FARZANA TASNIM

Submitted to the Graduate College of
The University of Texas Rio Grande Valley
In partial fulfillment of the requirements for the degree of

MASTER OF SCIENCE

May 2021

Major Subject: Chemistry

A STUDY OF NANOGENERATOR BASED FLOW SENSOR

A Thesis
by
FARZANA TASNIM

COMMITTEE MEMBERS

Dr. Mohammed Jasim Uddin
Chair of Committee

Dr. Jianzhi Li
Committee Member

Dr. Narayan Bhat
Committee Member

May 2021

ABSTRACT

Tasnim, Farzana, A Study of Nanogenerator Based Flow Sensor. Master of Science (MS), May 2021, 72 pp., 28 figures, 66 references.

The utilization of kinetic energy from fluid flow to power sensory systems is experiencing an all-time high research focus. Invention of nanogenerators have fueled this research focus with unprecedented flexibility of applications. Many studies have reported on utilizing the mechanism of nanogenerator for sensing fluid flow. In this short work, we have summarized different types of self-powered nanogenerator-based flow sensors and their applications. We have also classified the use of Nanogenerator based flow sensors in different fields, such as Bio-medical Application, Fluid velocity sensing, and Chemical Detection. In the Bio-medical field, the flow sensor can be used for the patient's infusion process and respiratory monitoring. In the fluid velocity sensing field, the flow sensor can work as a detector for the airflow and humidity percentage. The sensor can act as an anemometer (wind flow meter), Wind Vector Sensor, along with velocity measurement. In the reported chemical detection application, a nanogenerator was used to analyze the alcohol breath and measure the rising speed of bubbles of the coal bed. All these discussed flow sensors demonstrated the ability to scavenge energy while acting as a potential sensor. We further included that, most of the reported flow sensors are triboelectric, piezoelectric, and electromagnetic nanogenerator mechanisms. The hybrid system of nanogenerators was also reported. These engineered sensors can be the cutting-edge solution

for several problems on current flow sensing problems and future obstacles. In this work, a Rotating Sliding mode Triboelectric Nanogenerator (RS-TENG) was designed. Teflon (PTFE) tape was introduced to work as a tribo-negative layer and the copper sheet and copper tape were worked as an electrode, whereas the adhesive tape was used between two PTFE tapes to create multiphase TENG. This RS-TENG was fabricated to demonstrate the applications as a self-powered flowmeter for detecting wind speed. Also, in this thesis, we have included an experimental study of triboelectric nanogenerator bases self-powered flow sensors. The experimented flow sensor demonstrated a promising result and potentials to be used in industrial applications.

DEDICATION

The completion of my master's studies would not have been possible without the love and support of my family and friends. My mother DEWAN MOMOTAJ BEGAM, my father A. K. M. TASNIM, my sister REZWANA TASNIM, my two lovely daughters AYAAT & AMIRAH, and last but not the least, my husband AMINUR RASHID CHOWDHURY, wholeheartedly inspired, motivated, and supported me by all means to accomplish this degree. Thank you for your love and patience.

ACKNOWLEDGEMENTS

I will be always grateful to my advisor Dr. Mohammed Jasim Uddin for his invaluable supervision in scientific research and for encouraging me with infinite patience and relentless support instead of his limitations to complete my research work. He has been a great mentor for me. I am grateful to every single member of the Photonics and Energy Research Laboratory. I cannot defy the help from all Bangladeshi Students and Communities living in the Rio Grande Valley during my research period. I should mention especially Apu Deb, Md. Anis, MD Mashfiqur Rahman, Nizamul Nibir, Ali Zaker Shawn, Sanzida Kabir, Umma Nahar Zuthi, and Sharmin Emu for their support. I cannot defy assistance in my research from the previous lab member Abu Musa Abdullah. I would like to thank my friend Omusola for encouraging me. I am grateful to Ulises, Javiar, and Rafaqut for contributing to my research. I must mention my husband Aminur Rashid Chowdhury, who is the biggest and constant support for me during my stay and research in UTRGV. Without him, this journey wouldn't be easy for me. When I came to this country, I never had to think about the cultural gap because of these highly intelligent people.

I would like to also show my gratitude to the Department of Chemistry, UTRGV as well as the Dean's Office, College of Science, UTRGV for her support during my Journey of achieving the goal. I am grateful to Dr. Javier Macossay-Torres, Dr. Frank Dean, Dr. Evangelia Kotsikorou, Dr. Tülay Ateşin, Dr. Narayan Bhat, Dr. Karen Lozano, and Dr. Jianhi Li. I should

particularly express my gratitude to Dr. Parwinder Grewal (Executive Vice President, Office of the Executive Vice President for Research, Graduate Studies & New Program Development) for his support for my MS expedition in UTRGV. Financial support initiated by Dr. Grewal was a great backing for tension-free research. At last, I would like to thank the biggest support for me in this research work Dr. Mohammed Jasim Uddin, who has been mentoring me even before I arrived in UTRGV. His given flexibility made me think out of the box and utilize most of my potential. Without his support, this could have been next to impossible.

TABLE OF CONTENTS

Page

LIST OF TABLES

Page

LIST OF FIGURES

Page

CHAPTER I

INTRODUCTION

Internet of things (IOT) is one of nine important pillars for modern industrial revolution 4.0.[1] This interconnection of machines also referred to as IOT requires sensing intensive variables (color, temperature, luster, hardness, etc. and extensive variables; mass, size, weight, volume, flow rate, etc.).[2,3] Sensing extensive variables poses a greater threat to the safety and assurance of the whole system due to its complexity and change along with other parameters. Hence the requirement of ease of sensing extensive variables is crucial. Gas flow rate is one of the major extensive variables needed to be precisely measured for the betterment of the system.[4] Bulky sensors along with requirements of being powered by an external power source diminish many abilities of flow sensors to be used extensively to monitor and control industrials systems as well as day-to-day use devices.[5,6] A device that combines power sources along with sensory elements would greatly increase the working efficiency of different systems.

In today's world, it is impossible to think about our life without the sensors around us serving our every need.[7],[8][9], To fulfill these criteria, Z.L. Wang's group developed the first piezoelectric nanogenerator (PENG) based on the applied tension and charge separation across Zinc Oxide nanowires in 2006 [10]. This was the foundation for a wide array of self-powering[11],[12] and wireless sensors such as touch sensors[13],[14], magnetic sensors[15],[16], chemical sensors[17],[18], and flow sensors.[19,20] In 2012, Wang designed a triboelectric nanogenerator (TENG) that utilized materials of opposite charges to harvest energy at low cost[4]. The friction between both materials produced an electron flow that converts mechanical energy into electrical energy[4]. They serve as a promising alternative power source like wind turbines and solar panels. The demand for sustainable energy is rapidly increasing with the depletion of nonrenewable sources.[11,22,23] TENGs rely on the concept of electrification and electrostatic functions to produce energy by converting external forces into energy.[3],[24],[25] TENGs also have many flow sensor applications such as detection for air and breathing analyzer[26][27], health care monitoring of transfusion[28][5,29], water flow, and fluid velocity sensing[30][31][32]. Flow Sensors are unique in their design in the way that sensors detect the kinetic changes in liquid or gas. These sensors are self-sufficient, highly sensitive, environmentally friendly, and cost-effective. These highly sought out properties are of high importance for healthcare, environmental, and industrial fields.[19,30].

Figure 1 demonstrates the increasing trend in research (of) based on flow sensors. SciFinder and Web of knowledge were used for getting the data. According to the web of knowledge, a total of 175 papers have been reported on nanogenerator-based flow sensors. The

average citations of the papers are almost 50. This demonstrates the demand for research in this field.

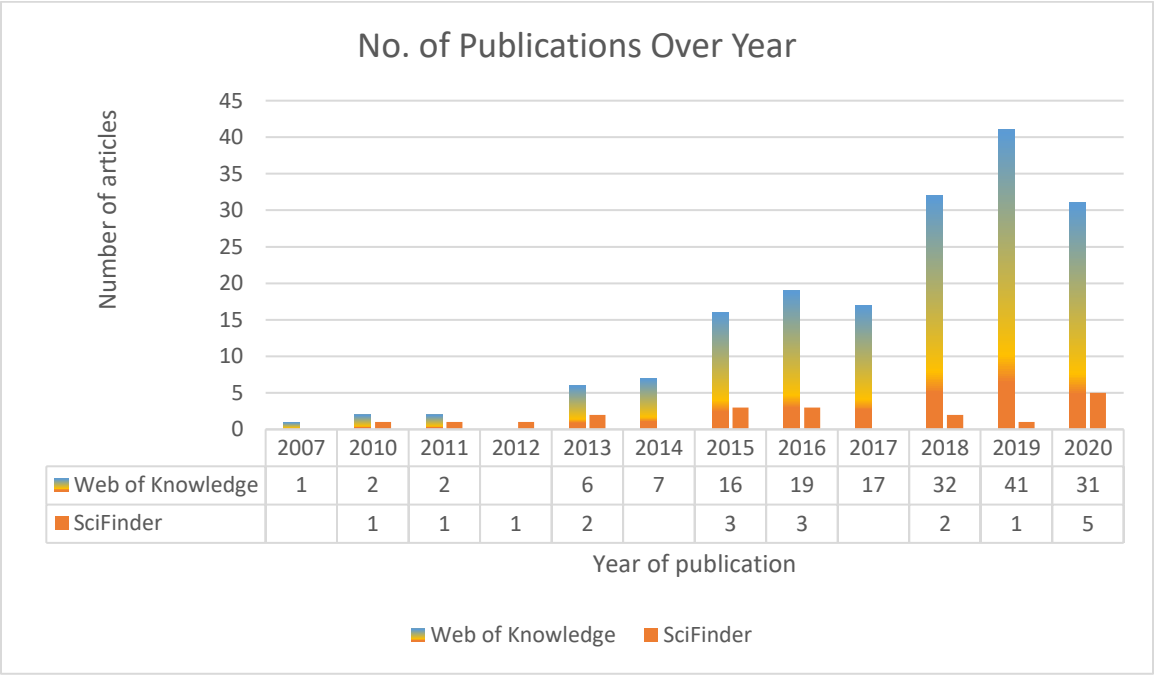

Figure 1: Researches in nanogenerator-based flow sensors over the years. The search keyword was “nanogenerator flow sensor”.

In this work, we present a self-powered triboelectric nanogenerator-based flow sensor. This flow sensor is a noble approach towards measuring the gas flow with high precision. Other than the effectiveness of the device’s ability to measure accurately the flow rate, the potential of generating electricity is also described. In addition to these, the flow sensor was connected to the microcontroller and demonstrated its ability to use it in a real-life scenario.

CHAPTER II

LITERATURE REVIEW

TENGs quickly proved to have fast response time with high sensitivity, which are great properties or flow sensors [33]. The first TENG air flow sensor in contact-separation mode was presented in 2013[33]. TENGs advancements led to the first two-phase TENG liquid and gas sensor in 2013 that detected water and ethanol. The air flow sensor detects wind vibrations and turns it into energy to fuel LEDs[33]. In that same year, the first PENG gas sensor was created to measure gas molecules absorbed on zinc oxide nanowires[34]. Shortly after in 2015, Wang designed the first hybridized flow sensor which measured temperature by harvesting air flow[35].

In 2007 Hu et al. created a wireless sensor node with hybrid energy harvesting applications. This TENG was a wireless solar power that allowed for solar panels and monitoring of temperature and environment monitoring[19]. In 2013, Yang et al. created a self-powered triboelectric nanogenerator that harvested wind energy. This device served as a wind sensor, vector sensor, and could even harvest wind energy from human blowing [36]. Additionally, Lin et al. created a piezoelectric zinc oxide nanogenerator that could sense wind speed and human respirator[34]. In 2014, Guo et al. produced a triboelectric nanogenerator that served as a humidity and air flow detector[37]. In 2015, Wang et al. created a TENG that could serve as a breath analyzer. This device was a blow-driven TENG that could sense alcohol, air speed, and air quality.[38] That same year, Alluri et al. created a self-powered piezoelectric film that served as

a fluid velocity sensor that power electronics[39]. Furthermore, Wang et al manufactured an aero-elastic flutter TENG that sensed temperature, airflow, and harvest energy from exhaling[35]. In 2016, Chan et al. created a self-powered microsensor that allowed for sensing gas and liquid flow. This microsensor could potentially monitor patient infusions in hospitals.[40] That same year, Sue et al., created a self-powered triboelectric flow rate sensor. This device could monitor the flow rate of wind and gas for energy harvesting.[41] The flowing year in 2017, Xu et al. created an aeroelastic flutter-based TENG that can be activated and self-powered by wind speed.[42] In 2018, Hu et al. created a wireless self-powered sensor node that could sense temperature, air condition, and flow rate.[28] Additionally, that same year Wang et al. created a wireless self-sufficient TENG that could monitor real-time respiration and harvest it into energy.[26] In 2019, Zhong et al. created an electromagnetic triboelectric hybrid nano generator. This device was a two-phase sensing and energy harvesting device.[43] In 2020, Zeng et al. created a triboelectric nanogenerator that had a highly efficient wind energy harvest and could monitor speed on flow-induced vibrations.[44] That same year Phang et all. Created a triboelectric aero-elastic flutter that is self-powered and could measure gas flow and wind speed.[45] Additionally, that year, Wang et al. produced a non-contact magnetic TENG that was self-powered and could determine water level and liquid velocity.[30] Later that year Chang et al. created a self-sufficient triboelectric spherical sensor for fluid velocity detection and environmental monitoring.[46] That same year Fan et al. developed a two-phase TENG that allowed flow pattern sensing and could sense coalbed methane and bubble detection.[47] Furthermore, in 2020, Wang et al. developed a multi-functional wind barrier that was self-powered and could sense wind speed from passing vehicles while harvesting energy.[48]

Developed by Wang in 2013, triboelectric flow sensors have been great advancements in triboelectric nanogenerators.[36]

Figure 2: Timeline for different types of Flow Sensors

Flow sensors are composed of either triboelectric, piezoelectric, or hybridized materials. The majority of the flow sensors consist of triboelectric sources. From those flow sensors, various things are measured, with the most common flow sensor which measures gas or air. Other than that, the liquid, temperature, and two-phase fluid can also be measured by the flow sensors. Development in TENGs continues due to their various benefits such as ease of production, low cost, and efficient power output. The need to increase the power output and efficiency of nanogenerators led to the idea to mix TENGs with PENGs and other nanogenerators. This concept was known as hybrid sensors or hybridized Nanogenerator[49][50].

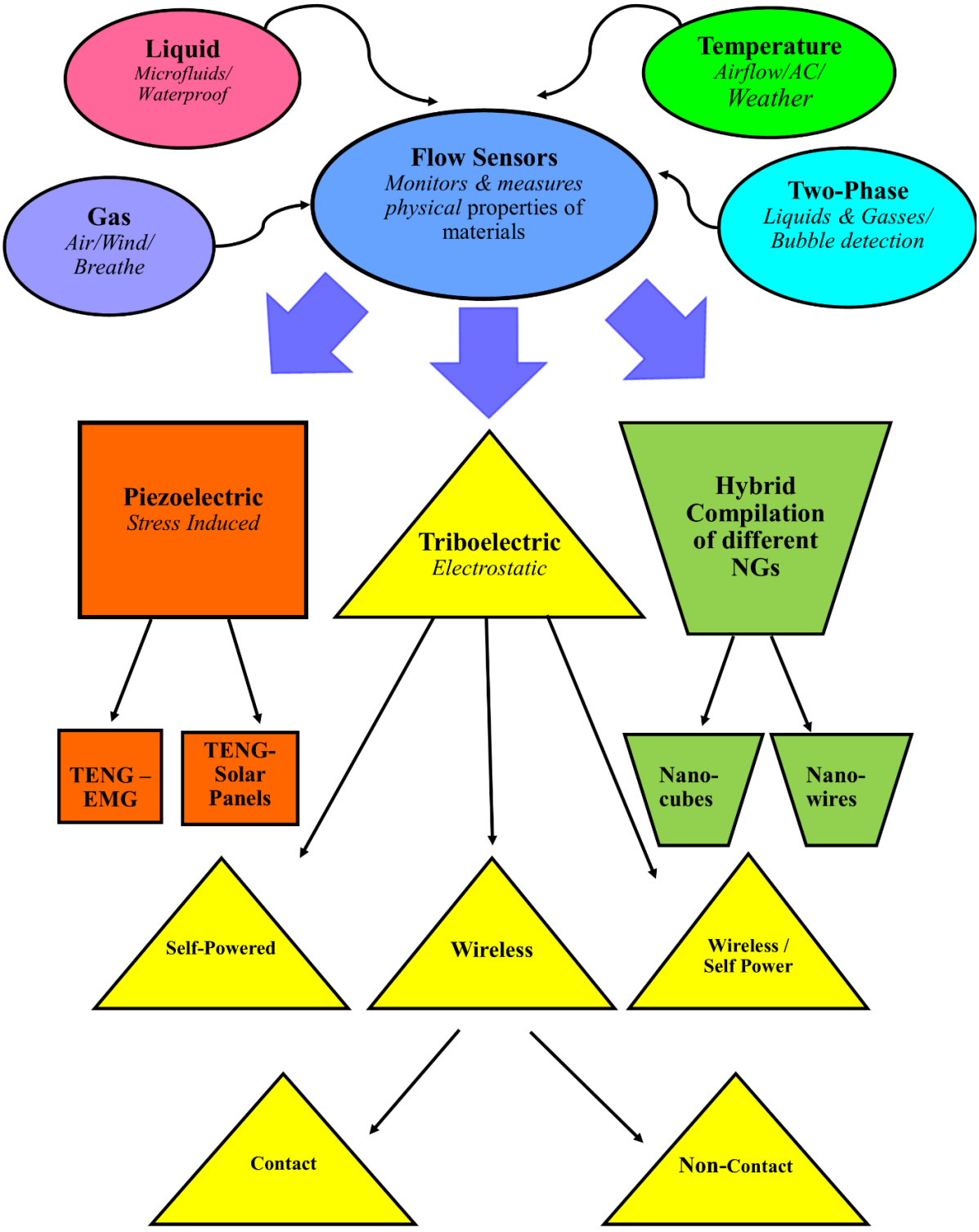

Figure 3: Types of Flow Sensor

Bio-Medical Application Based Flow Sensor

Chen et al.[51] has proposed a self-powered triboelectric microfluidic sensor (TMS) by utilizing the electric signal produced from the droplet/bubble via the capillary and triboelectrification of liquid/solid interface for real-time liquid and gas flow detection. Their work is optically and schematically demonstrated in figure 5. This TENG works on single-electrode mode and is compatible to detect frequency for both water and air flow. In this research, the flow rate and flow volume are calculated by the interval time between two signals and accumulating the signal number in a certain interval time. The range of detection and sensitivity is depended on the diameter of the capillary. The TENG is consists of a polyethylene (PE) tube as the substrate, polytetrafluoroethylene (PTFE) as the tribo-layer that modifies the internal surface of the PE tube with hydrophobic and electret properties, and the copper layer as an electrode on the outside surface of the PE tube.

In the case of the liquid flow sensor (Figure 4a), droplets are detached from the tip of the capillary passing through TENG area, whereas, in the case of the gas flow sensor (Figure 5b), bubbles grow on the tip of the capillary going through the TMS area so that voltage signal is induced. The working principle of Liquid-TMS starts with the positive electrode under short-circuit condition due to the electrostatic induction effect and will establish a negative potential difference to the ground at the beginning of the triboelectric charge transfer. When the negatively charged PTFE comes in touch with the water droplet, it forms an electric double layer (EDL) that must screen the electrostatic induction of negatively charged PTFE to the overlapped electrode. As a result, electron starts flowing from the ground to the Cu electrode. At the end of the circle, the screen effect will disappear, and the overlapped electrode will be reduced by positive charges

under short-circuit condition and re-establish a negative potential difference between electrode and ground, as depicted in Figure 5a. When this cycle starts working periodically, intermittent output signals are recorded.

The Gas-TMS is effective when air bubbles break the screen effect of EDL due to the screening of the electrostatic induction on the overlapped electrode. The negative charge on the PTFE surface will induce the overlapped electrode to be positively charged, where the negative potential difference between the Cu electrode and ground drives electrons to flow from the electrode to the ground and reach an electric equilibrium. As soon as the air bubble escapes from the PTFE surface, the EDL will be reformed, where the electrons flow from the ground to the electrode to neutralize the positive charges on the electrode. This research work shows a linear relationship between the output frequency of TMS and the flow rate on different capillaries. The smaller capillaries show greater sensitivity and the larger ones show a relatively wider detecting range. The Liquid/Gas-TMS could be applied as a real-time monitor for patient's infusion process in hospitals and industrial field to detecting gas flow to realize the self-powered system (Figure 5 e & f).

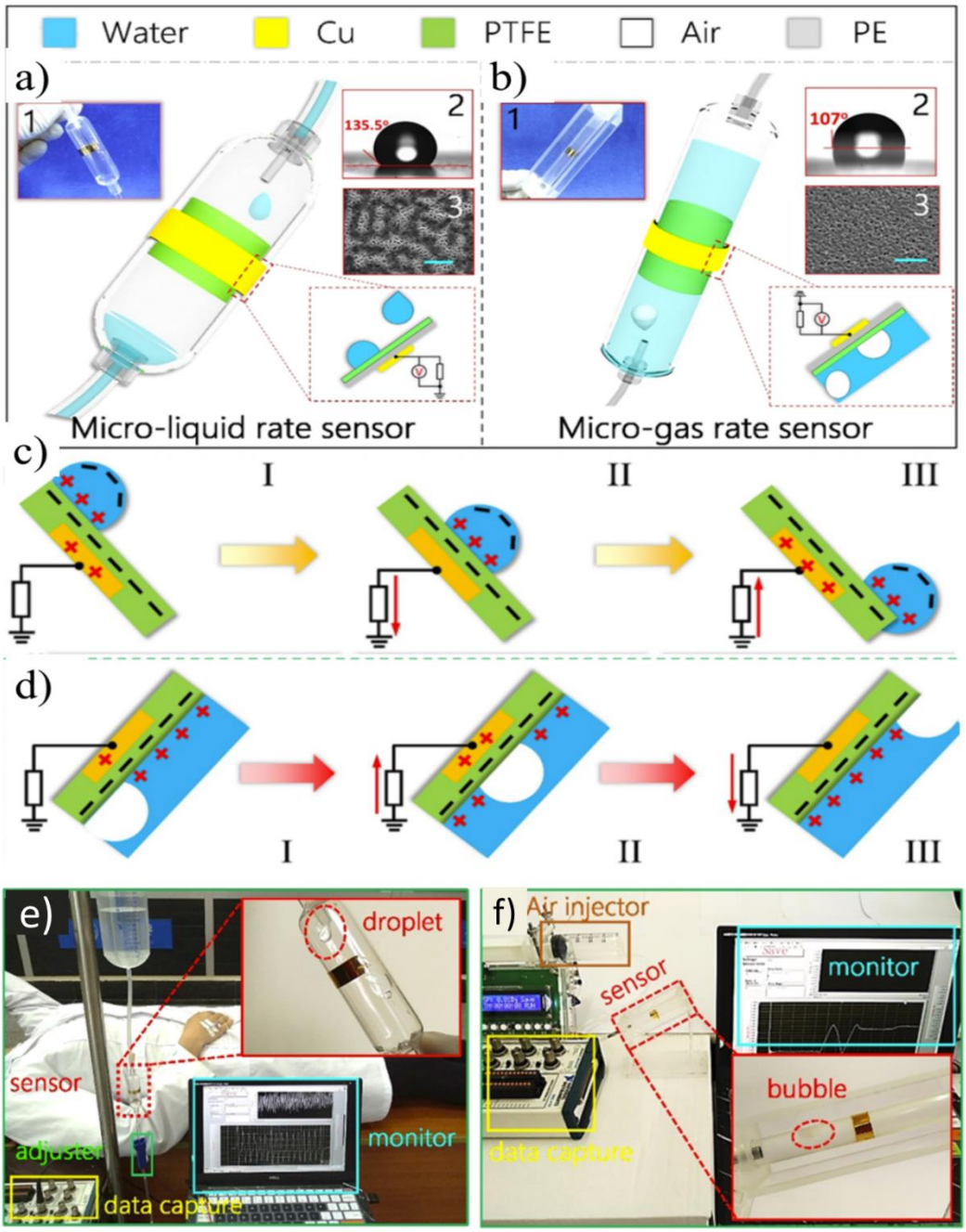

Figure 4: Schematic representation of the structure of the a) liquid flow rate sensor, b)gas flow rate sensor (c) & (d)Working mechanism of the flow sensor e) Infusion monitor using the liquid flow sensor f) Gas detector with the gas flow sensor. [51]

Lin et al[34], discussed a piezoelectric ZnO nanogenerator that works as a wind speed sensor using the hydrothermal method (Demonstrated in Figure 5). They claim that this highly flexible and lightweight sensor can be used for human respiration detectors since it shows high sensitivity to air flow with a rate of 0.5 ms^{-1}. For a wind speed sensor to detect air flow rate from human respiration, the cut-in wind speed of the sensor should be less than 2.0 ms^{-1} or even more. The fabrication is done by the ZnO nanowires embedded in the PDMS layer by spin coating.

A respiratory machine (Respironics Lifecare PLV-100) was used to conduct the experiment for human respiration. The ZnO nanogenerator was placed inside the external pipe which is connected to the respiratory machine and a test lung to mimic the normal human respiration behavior. During inhalation, the air flows from the respiratory machine to the test lung in the pipeline, swaying the device in the direction of the test lung. During exhalation, the device sways in the direction of the respiratory machine. During inhalation and exhalation, the ZnO nanogenerator swaying generates the different piezoelectric potential of NWs, then induces the opposite charges on the surface of the top to bottom electrodes. To minimize leakage, only one external pipe connector was used to link the respiratory machine and the test lung.

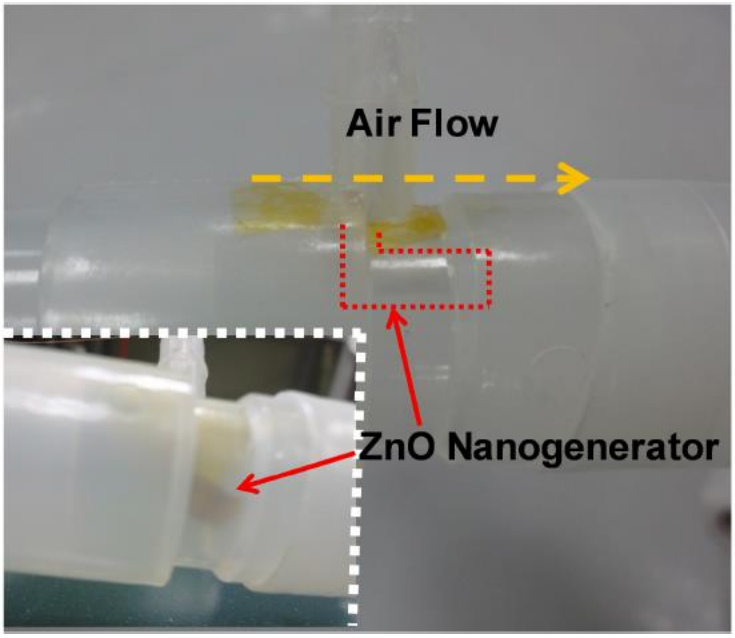

Figure 5: Optical representation of the ZnO nanogenerator with swaying (backward and forward) action during respiration inside the external pipe connector. The bending angle was approximately 90°. side view of the swaying action(inset). [34]

In this experiment, the open-circuit voltage is counted 41mV for normal human respiration at rest while the tidal volume is 500 mL and the air flow rate is 2.0 ms^{-1}. The maximum open-circuit voltage and closed-circuit current-density can be observed at the air flow rate of 5.0 ms^{-1}, 61.2 mV, and 7.12 $nAcm^{-2}$, respectively. It is also proved that if the tidal volume & air flow rate, the electrical performance also increases, such as 81.3 mV and 11.4 $nAcm^{-2}$ was recorded at an air flow rate of 2.0 ms^{-1} .

Wang et al. [35] has worked with an elasto-aerodynamics-driven triboelectric nanogenerator (TENG) for Scavenging Air-Flow Energy based on the contact electrification method. The device structure is shown in figure 6 below. This device shows the concept of harvesting the human breath-induced air-flow energy for sensing body temperature effectively.

The device is fabricated by a Kapton film with two Cu electrodes at both sides and two polytetrafluoroethylene (PTFE) films with Cu electrodes at the top and bottom acrylic substrates. The Kapton film is fixed at the middle of the device and with two narrow air gaps created between the PTFE films and the Kapton film.

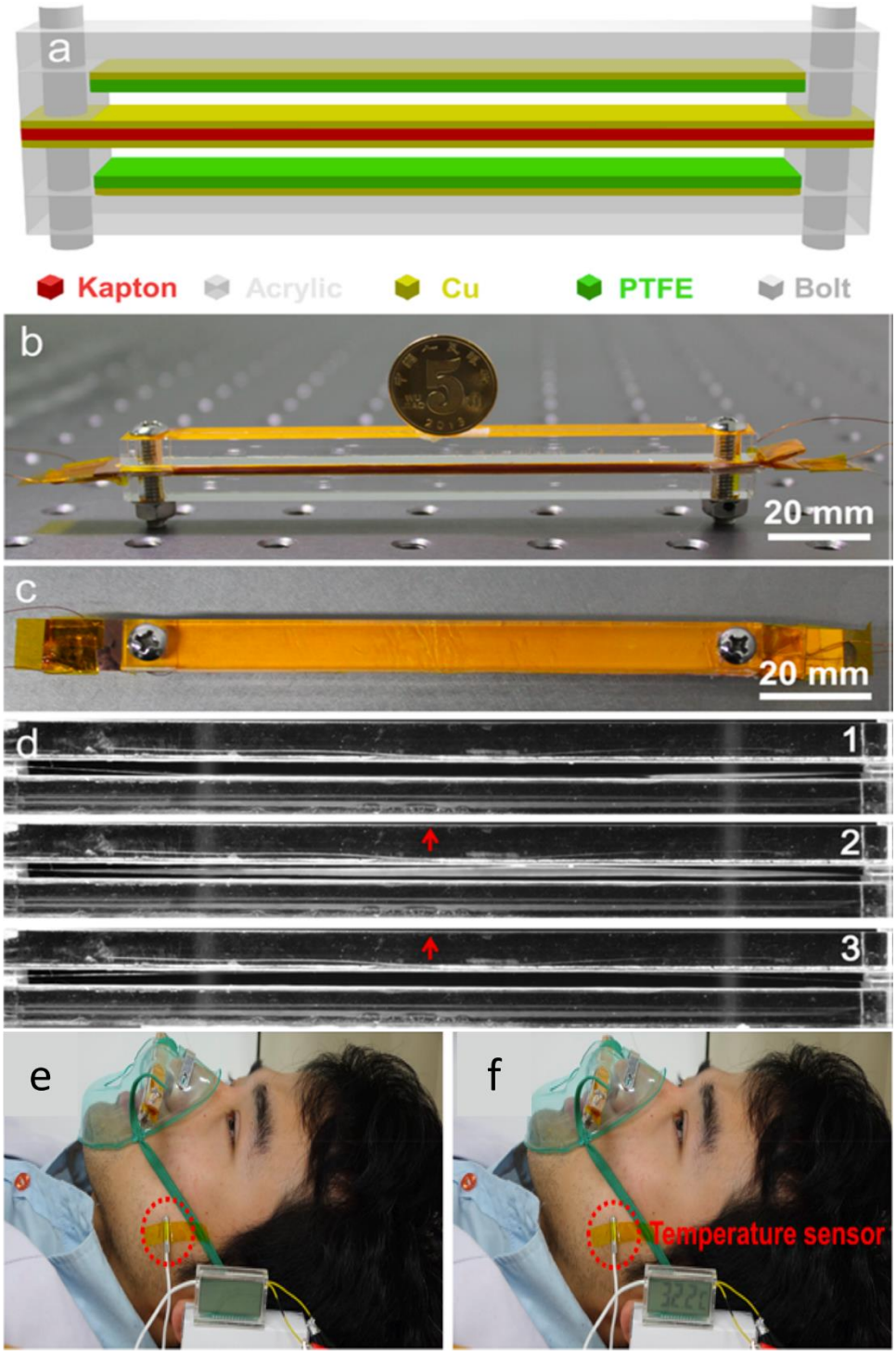

Figure 6: (a) Schematic representation of the fabricated TENG. (b) The cross-sectional optical picture of the fabricated TENG. (c) Top (optical) view of the fabricated TENG. (d) Optical picture of TENG in high-speed motion (e and f) Optical photograph of using the TENG to

scavenge human breath induced air-flow energy to sustainably power a temperature sensor system. [35]

The TENG is activated by periodic contact and separation of the Cu electrode and Kapton film and PTFE film. The coupling between triboelectrification and electrostatic induction results in the alternating flow of electrons between electrodes. Once the inlet wind speed approaches the critical wind velocity of the Kapton thin film, the damping ratio of the twist motion will be decreased to zero and thus start the fluttering of the Kapton film. The flutter phenomenon enables the vibrated film to extract energy from the free wind flow when there is a phase difference between film structure instantaneous aerodynamic force and the elastic deformation. Once the inlet wind speed approaches the critical wind velocity of the Kapton thin film, the damping ratio of the twist motion will be decreased to zero and thus start the fluttering of the Kapton film.

The top TENG shows the output performance of 240 V output voltage and about 80 μA short-circuit current and 3 kW/m^3 as the largest power density, whereas the bottom TENG shows 220 V, 60 μA, and 2 kW/m^3 respectively. The experiment shows that the output voltage is directly proportional to the air gap (the distance between the top and bottom PTFE films), where the working frequency of the device holds an inverse relation with the increasing width and length of TENG. At the same time, the power density is also proportional to the length of the device. The largest output voltage is observed in the device with a width of 10 mm, which corresponds to a larger output power density of 3 kW/m^3. The lifetime of the TENG depends on the durability of Cu electrode on the Kapton film under the vibration process, where the potential

improvement can be achieved by improving the adhesion of Cu electrode on the Kapton film. They claim that there is no significant damage to this device even after 4.1 $x10^6$ cycles. It can be found that the total output current of TENGs dramatically increases with increasing the number of devices. They demonstrated a self-powered temperature sensor system that monitors the temperature of the human body with this TENG by inducing human nasal breath. As a sensor, the output current and voltage is shown be up to 30 V and 18 μA under a loading resistance of 2.3 MΩ, respectively, resulting in output power of 0.75 mW.

Wang et al [52] has discussed a flexible and low-cost air-flow-driven triboelectric nanogenerator (TENG) for self-powered real-time respiratory monitoring by scavenging mechanical energy of human respiration and transforming it into electric output signal using periodic contact-separation mode. The structure of the TENG is demonstrated on figure 7. The TENG is composed of a large number of nanofibers intertwined based n-PTFE to create high porosity and extremely large surfaces inside and on the surface of the PTFE film. Cu is used as an electrode and is attached to the top side of the n-PTFE. One side of the n-PTFE film is attached to the middle of an acrylic tube. Another Cu film is involved with the bottom surface of the acrylic tube. When air flows into the acrylic tube, the PTFE thin film could be agitated to oscillate and make constant contact/separation with the bottom Cu electrode in the acrylic tube.

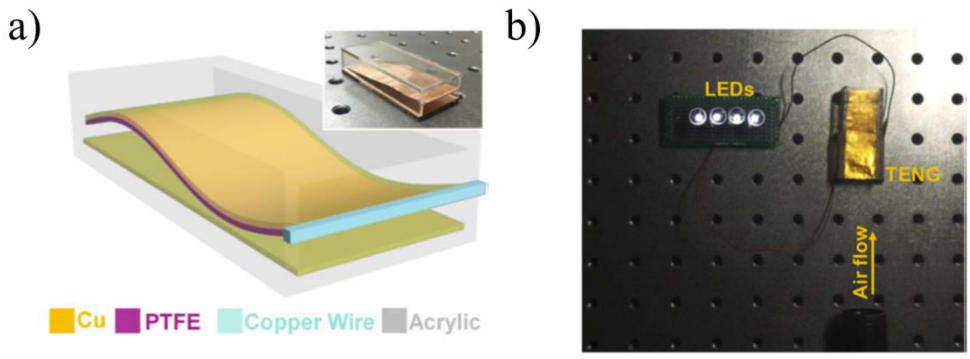

Figure 7: (a) Schematic representation of the configuration of the air-flow-driven TENG. optical photograph of the TENG device (inset). b) LEDs powered by air-flow-driven TENG (flow rate 120L/min). [52]

The electrical performance varies from 1.7 V to 11.1 V for output voltage and 0.9 μA to 10.2 μA for output current while the airflow rate rose from 85 L/min to 216 L/min. They proved the device can deliver an appropriate response even under highly humid conditions during normal human respiration by increasing the humidity from 50% to 90%. The average peak values of output voltage and current decreased from 1.5 V to 0.4 V and 0.8 μA to 0.2 μA, respectively. When they tested with the capacitor (4.7 μF) it showed 19.9 V in 150 s under an air flow rate of 216 L/min. They have also demonstrated the electric energy generation of the TENG by lighting up four commercial white LEDs under an air flow rate of 120 L/min.

Fluid Velocity Based Flow Sensor

Alluri et al, [39] have developed a Self-Powered Fluid Velocity Sensor by using a flexible and eco-friendly Piezoelectric Nanogenerator(PENG) made of highly crystalline $BaTi_{(1-x)}Zr_xO_3$ nanocubes (abbreviated as BTZO) embedded into a polyvinylidene fluoride (PVDF) matrix. The PVDF and 25 wt % of $BaTi_{(1-x)}Zr_xO_3$ were mixed by ultrasonic process and then dried to make a Piezoelectric polymer film. The Al was attached to both sides of the film to complete the nanogenerator structure. Cu wires were attached with silver paste on the top and bottom of the Al-coated hybrid film for Electrical connections. Polydimethylsiloxane (PDMS) was used as a packaging layer for the NG to protect the device from external conditions, such as mechanical stress, temperature, and humidity. The fabrication of the nanogenerator is demonstrated in figure 8.

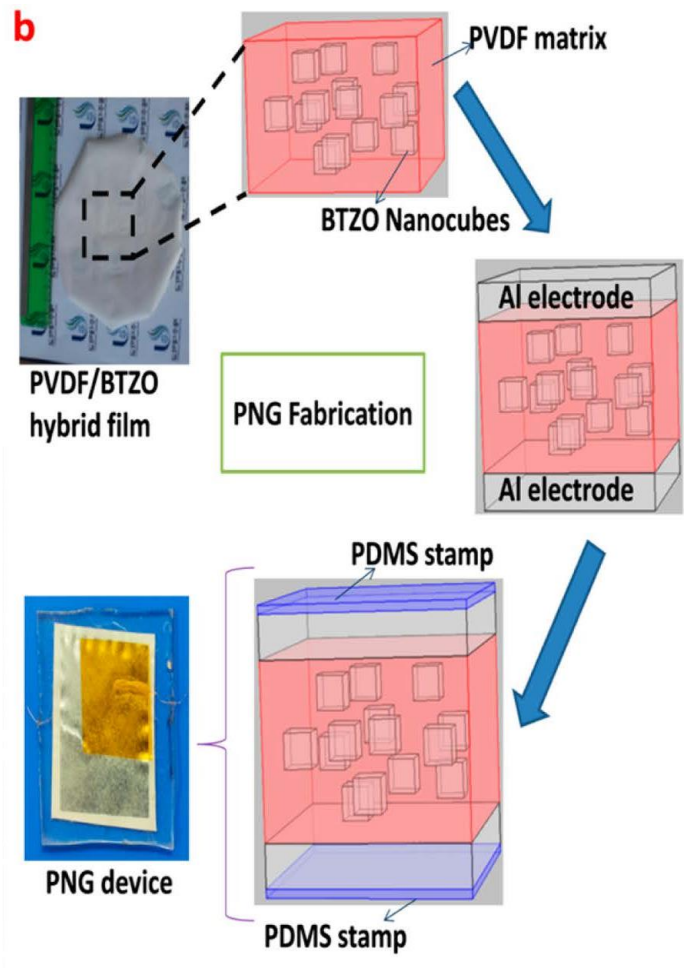

Figure 8: Schematic representation of key steps during the fabrication of a BaTi0.9Zr0.1O3/PVDF PENG device. [39]

This PENG was placed on a fixed support perpendicular to the direction of the water flow by covering with a polyethylene (PE) to avoid direct friction of water and PENG and a rotating faucet with two conditions, water ON and water OFF, over periodic time intervals was attached to control the water velocity. During the water ON condition, the electron moves across the top & bottom surface, resulting in potential differences with different polarities that were generated in the same plane as the NG. During the water OFF condition, the induced charges return to their

initial state. During the water ON condition, the average electrical performance of PENG at a water velocity of 31.43 m/s is mV for output voltage and 8 nA for current. , In the same circumstances, the water OFF condition shows 80 mV and 10 nA for the voltage and current, respectively. Upon increasing the water velocity from 31.43 to 78.6 and to 125.7 m/s, the corresponding output voltages and currents reached 213 and 466 mV and 19 and 34 nA, respectively, during the water ON condition. The total power produced by this device PENG varies from 0.2 to 15.8 nW for water velocities ranging from 31.43 to 125.7 m/s during the water ON condition. The PENG shows high sensitivity in both ON & OFF conditions as the small amount of water droplets restrict the transient charge carrier motion. This sensor can be used industrially for pump monitoring, process control, and HVAC (heating, ventilating, and air conditioning).

Guo at el. [53] have discussed an airflow-induced triboelectric nanogenerator (ATENG) with the FTO conductive glass and PTFE (demonstrated in figure 9), which works as a self-powered sensor to detect high humidity and airflow rate. The triboelectric part is fabricated by fixing the two ends of PTFE with each electrode using kapton tape with a conductive surface inside. Airflow is produced by a structure made of a rubber sleeve and a PE tube.

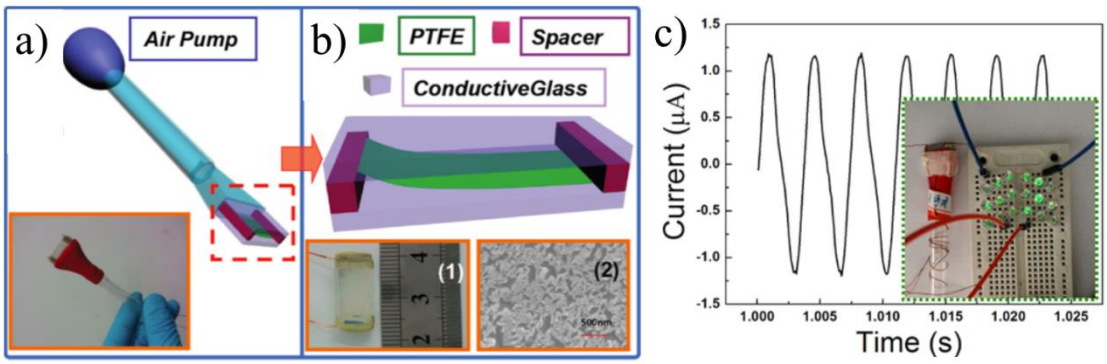

Figure 9: a) Schematic representation and optical photograph (inset) of the designed ATENG sensor. b) Enlarged view of the area indicated by the dashed red box in panel a, Optical photograph of ATENG, and (b, inset 2) SEM image of the surface of PTFE film (inset). c) Output current curve of the sensor and digital photograph of LEDs powered by the ATENG (inset). [53]

In this experiment, they proved that the faster the Flow Rate is, the higher the output current. On the other hand, the Relative Humidity holds an inverse relation with the short current. The highest value of the short current is 4.2 μA, which is achieved at 20% Relative Humidity. Due to the signal closing to background noise, they chose the output current of the external environment Relative Humidity, which is less than 80%, as the detection variable for Flow Rate instead of the 100% Relative Humidity. When the Relative Humidity reaches a certain value (>80%), the PTFE film adsorbs many of the water molecules that shield the charges on the film and lead to a clear drop trend with a decrease in Flow Rate. This research shows that the output voltage and short current can be used as detection variables for a self-powered humidity sensor, but for a self-powered airflow rate sensor, only the output short current can serve as a detection variable because the output voltage is not in monotone change with respect to flow rate. They were able to lit up 18 LEDs simultaneously, with an output short current of 1.25 μA.

These ATENG devices can be used as self-powered sensors for environmental monitoring and industrial manufacturing with advantages of self-power, multifunction, low cost, simple fabrication, and high sensitivity.

In another work, Su et al [54], worked with a segmented triboelectric nanogenerator (shown in figure 10) (STENG) for scavenging wind energy to work as a self-powered flow rate sensor. This STENG is composed of fluorinated ethylene propylene (FEP) and copper (Cu) foil acting in dual roles of electrode and contact surface. Processed FEP film was etched through inductively coupled plasma (ICP) to create a nanowire structure on the surface to increase the effective contacting area and triboelectric charge density in the friction process. This STENG follows the free-standing mode by fixing one side of the FEP fixed to the supporting beam, leaving the other end free-standing. When air flow starts, the FEP film periodically changes its distance with Cu, as a result, electricity is produced. This segmented structure is able to effectively inhibit the inner counteraction resulting from the diverse electric potential of the oscillating film. This device shows an output of up to 36 V open-circuit voltage and 11.8 μA short-circuit current. It is also able to trigger 20 LEDs under a wind flow rate of 17.9 m/s, and a charged capacitor of 30 μF with a maximized output power of 114.7 μW. They proved that the output voltage holds a proportional relationship with the loading resistance, whereas the output current shows the opposite trend. The maximal output power is 114.7 μW with a loading resistance of 300 MΩ. They claimed that this STENG performs linearly for the electrical output with wind speed which can make it a self-powered triboelectric sensor in wind energy harvest, self-powered gas sensor, gas flow monitor, and high attitude navigation.

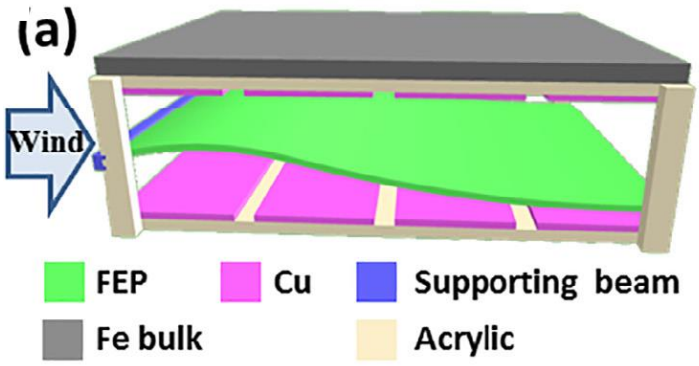

Figure 10: Schematic representation of the Single-electrode-based segmented triboelectric nanogenerator (STENG). [54]

Xu et al [42], produced an aeroelastic flutter-based triboelectric nanogenerator (AFTENG) that works as a self-powered active wind speed sensor by measuring the fluttering frequency instead of the output voltage/current.

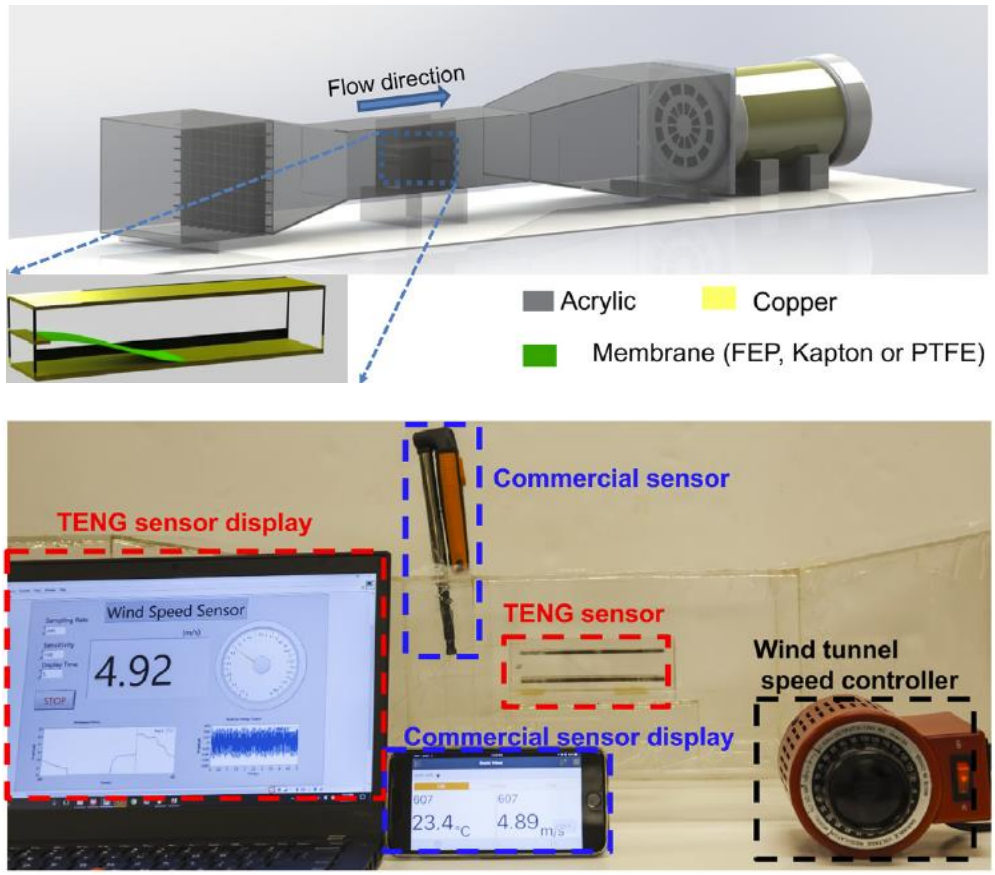

Figure 11: a) Schematic representation of a wind tunnel and the structural design of AFTENG with an acrylic tube. b) Comparative optical picture of the application of the real-time velocity measurement using AFTENG wind speed sensor and a commercial sensor. [42]

The structure of the AFTENG is shown in figure 11. This AF-TENG is made of two copper layers as an electrode and different membrane materials, including fluorinated ethylene propylene (FEP), polytetrafluoroethylene (PTFE), and Kapton in a cuboid acrylic channel. The working principle of the AFTENG is based on the coupling of contact triboelectrification and electrostatic induction. When the wind flow is introduced to the tube, the membrane starts moving vertically periodically due to the fluttering effects. At the same time for

triboelectrification, charge produces and preserves on both electrodes due to the nature of the dielectric material.

The fluttering frequency is better for the thinner FEP than the thicker FEP membrane. The wind speed is proportional to the contact force between the fluttering membrane and electrode. As the contact force becomes high, the surface charge density would also be high. The largest output that comes from this device is 6 V open-circuit voltage and 9 μA current (approx.) at a wind speed of 9.2 m/s.

To prove the wind speed sensor capability of the AF-TENG , this device was compared to a commercial hot-wire anemometer (Testo 405i) and by analyzing it was found to be compatible for real-time wind speed measurements. The corresponding speed sensitivity was found about 0.13 (m/s)/Hz or 7.7 Hz/(m/s). This proves the AFTENG can be used in wireless environmental monitoring networks, even in high humidity environments.

Though there have been many studies involving small-scale operations of TENGs, there have not been many large-scale applications of TENGs. Wang et al [48], proposed a triboelectric nanogenerator (TENG) which can work simultaneously as a self-powered wind speed sensor and highly efficient windshield. This multifunctional device is fabricated by two copper electrodes and one strip of fluorinated ethylene propylene (FEP) membrane fixed in a 3D printed polylactic acid (PLA) channel. The electricity generation from this TENG occurs by the freestanding contact mode with the dielectric membrane fluttering between two electrodes.

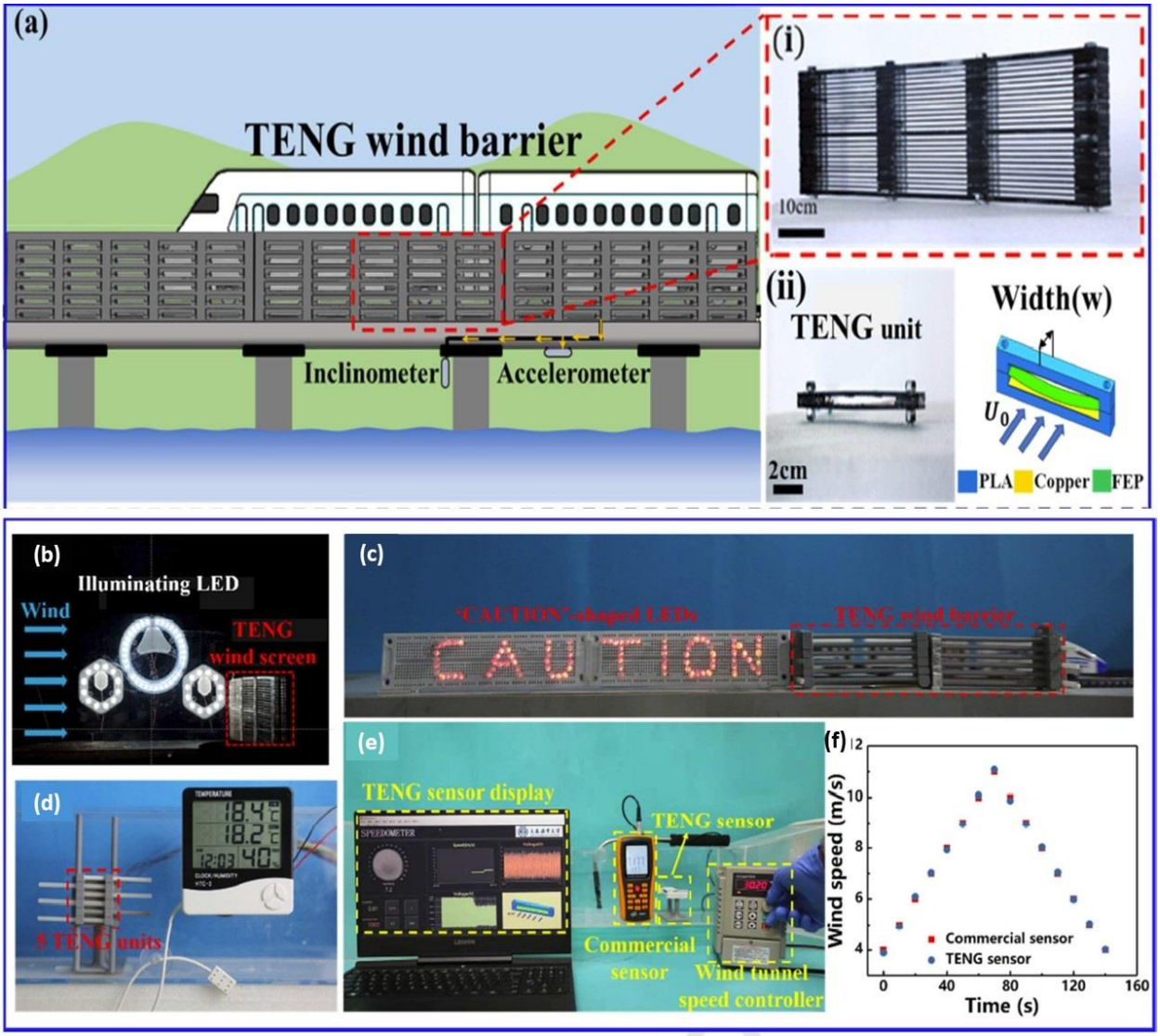

Figure 12: Optical representation of (a)application scenario of the TENG-based wind barrier, photograph of the TENG unit, and schematic diagram of the TENG unit. TENG-based wind barrier as a power source and a sensor powering (b)household illuminating LED, (c) 'CAUTION'-shaped LED lights and (d) a temperature and humidity sensor by the TENG-based wind barrier. (e) The optical view of the real time wind speed measurement using the TENG

sensor and a commercial sensor. (e) Comparison of the response of TENG sensor and commercial wind speed sensor. [48]

They claimed the TENG (in figure 12) unit performs the best when the wind blows vertically. The highest electrical output of this TENG is achieved at a wind speed of 10 m/s, corresponding to a maximum current of about 11μA, a maximum output power of 5.9 mW under the matched loading resistance of 100 MΩ. A group of 66 TENG units connected in parallel was used as the wind barrier which can produce an output power of 26 mW and current of 440 μA under the loading resistance of 1 MΩ at the wind speed of 10 m/s. A linear relation was obtained for the critical wind speed and the TENG width. This TENG can scavenge the slipstream energy induced by passing vehicles. The author also claimed that this wind barrier is 35% more efficient than that of the traditional porous wind barrier. This TENG can also be used as a self-powered anemometer to monitor the condition of the wind barrier.

For practical demonstration, they showed several applications including directly lighting the LED at the wind speed of 10 m/s. The 'CAUTION'-shaped LEDs lit up by the TENG-based wind barrier, whereas a temperature and humidity sensor powered by 5 TENG units connected in parallel at the wind speed of 10 m/s, and the TENG sensor comparison with a commercial anemometer.

Zhong et al,[43] has assembled an Electromagnetic-Triboelectric Hybrid Nanogenerator (EANG) as a self-powered flow sensor to harvest fluid energy. Here they used magnetic coupling for the ease of encapsulation, installation, and maintenance along with the goal of reducing friction by soft contact between the triboelectric film and the electrode. This device is implemented by a cylindrical stator with Cu foils to the inside surface as electrodes, Cu coils

fixed on the inner surface of the stator, and a cylindrical rotator with FEP films on the outer surface as a triboelectric layer, and magnets in the top & bottom of the rotator. The hybrid nanogenerator works as a sliding freestanding mode TENG and a rotary electromagnetic generator (EMG). When the FEP blades touch the first electrode the electron starts flowing from Electrode I to the FEP film due to the triboelectrification effect. When the rotator starts moving, the electron starts to flow from the second electrode to the first electrode through an external circuit to maintain the electrostatic equilibrium between the two electrodes. When the FEP comes in contact with the second electrode, the reverse action happens. They claimed that the electron flow occurs due to the potential difference between Electrodes I and II. The EMG follows Faraday's induction law and generates electricity by coupling with magnet & Cu coil while rotating.

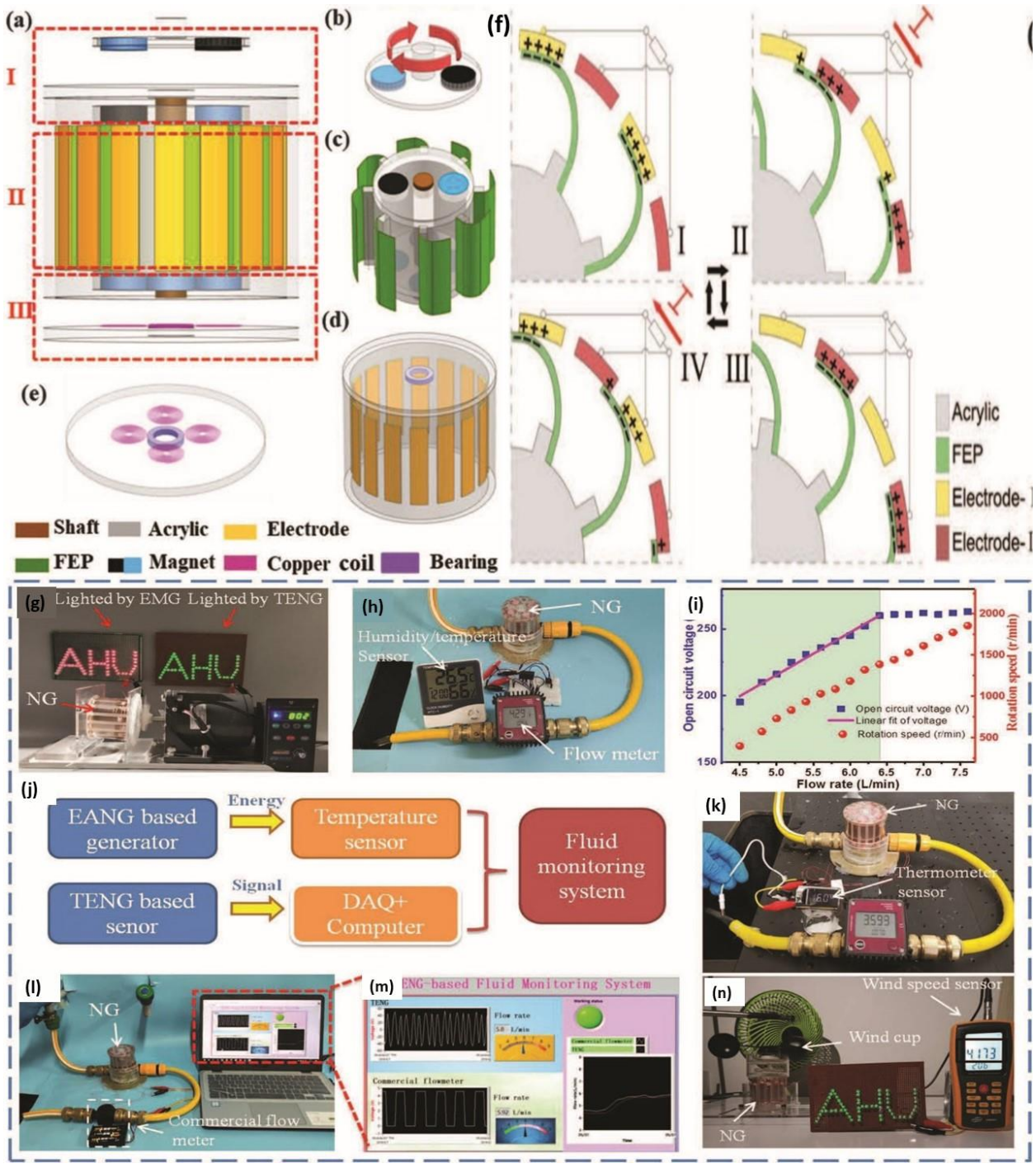

Figure 13: Structural design and application of the hybrid nanogenerator in a smart home. a) Schematic diagram of the designed hybrid nanogenerator, including a magnetic coupling (I), a sliding freestanding mode TENG (II), and an EMG (III). b) Driving part of the magnetic

coupling. c) Rotator of the NG (i.e., the follower of the magnetic coupling). d) Stator of the NG with the upper cover. e) Lower cover of the stator with four coils and one bearing. f) Scheme of the working mechanism of the TENG. g) Photograph of red and green LEDs lit by the individual EMG and individual TENG driven by a motor. h) EANG to harvest ting water flow energy to power a humidity sensor. i) Relationship between the open-circuit voltage of the TENG, rotating speed, and flow rate. j) System diagram of a self-powered fluid monitoring system. k) Photograph of a thermometer sensor successfully driven by the EANG to detect the water temperature. l) Photograph of the measurement platform to compare the detection ability of the EANG and the commercial flow meter. m) Real-time fluid monitoring interface programmed by LabVIEW software. n) Photograph of the NG harvesting wind energy and lighting LED arrays at a wind speed of 4 m s^{-1}. [43]

They showed for this device that the Voc and Qsc increase proportionally with the rotation speed. The TENG has the maximum output voltage of 48 V and load power of 1.05 mW at a rotating speed of 500 r min^{-1} under a load resistance of 4 MΩ, whereas the EMG has the maximum output voltage of 4.8 V and load power of 58.3 mW under a load resistance of 20 Ω. The durability test of the TENG was done at a rotation speed of 500 r min^{-1}. This hybrid TENG and EMG setup was able to light up 61 green and 61 red LEDs arranged into “AHU”. The EANG can be used to harvest fluid energy and work as a self-powered flow sensor to detect the flow rate of water using a fluid monitoring system in a real environment

Yang et al. [55], established a Triboelectric Nanogenerator that can work as a wind energy harvester as well as a self-powered wind vector sensor system for wind speed and direction detection. The device is composed of Al film in the top and bottom side of a cuboid

acrylic tube and the Fluorinated ethylene propylene (FEP) film in the middle attached with a copper wire by one side and free-standing on the other. The device was tested under a uniform air flow of 10 m/s by an air gun and the developed voltage and current are about 5 V and 0.5 μA under a loading resistance of 100 MΩ, respectively. When a bridge rectifier is connected parallelly the output voltage boost up to 100 V, output current becomes 1.6 μA, and an output power shows up to 0.16mW under a load of 100 MΩ.

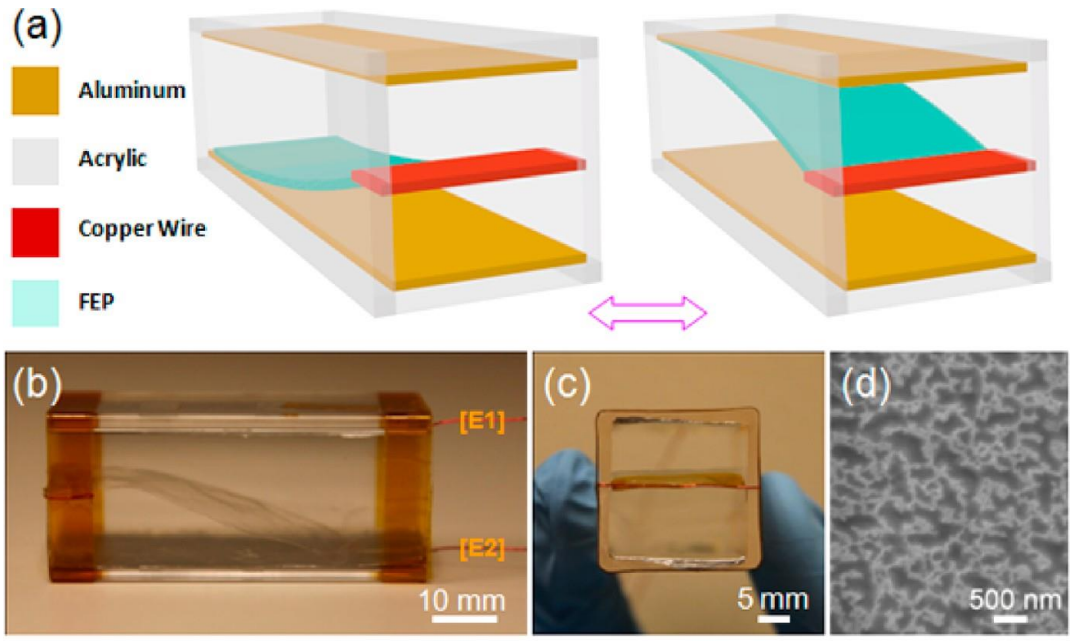

Figure 14: (a) Schematic diagram of the TENG. (b) Side optical view of the TENG, (c) Side optical view of the TENG,. (d) SEM image of the etched FEP film surface. [55]

The nanogenerator was fabricated with an additional double-electrode-based TENG which works as periodic contact/separation mode (in figure 14 and 15). This wind-sensitive unit is fabricated by a copper electrode, a polytetrafluoroethylene (PTFE) film, and an Al electrode on a Kapton film. The measured largest open circuit voltage is 110 V and short-circuit current of the TENG is about 80 μA. under a wind speed of about 10 m/s. The TENG was able to light up 10 LEDs by harvesting only the wind energy induced by blowing.

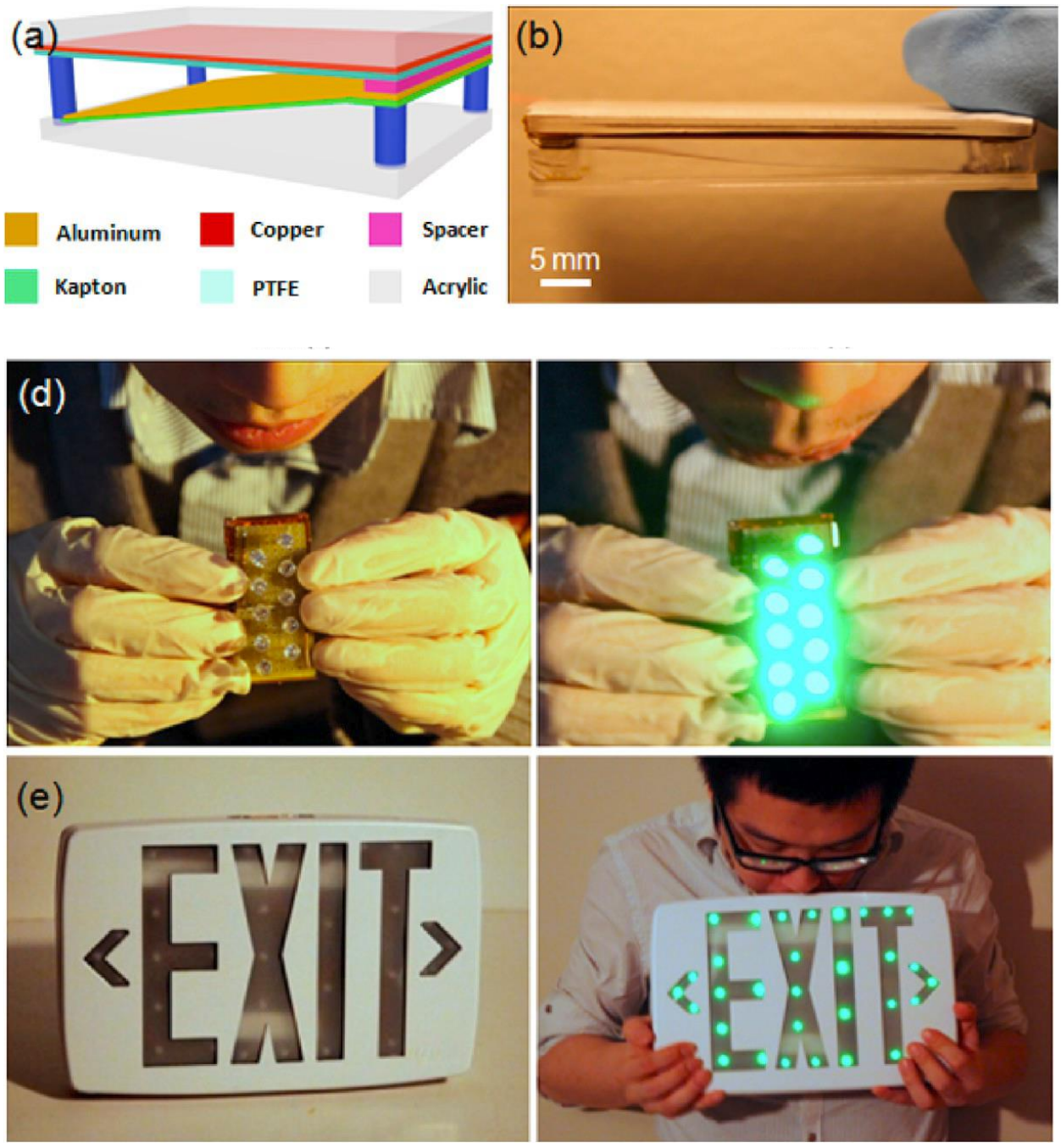

Figure 15: (a) Schematic representation of the designed double-electrode-based TENG. (b) Optical representation photograph of the TENG. (d) & (e) Optical Photographs of TENG to harvest the human mouth blowing induced wind energy to drive 10 LEDs and exit sign[55]

For testing the TENG as an active wind vector sensor, four TENGs resided along with four directions, where Each electrode was connected with a loading resistance of 20 MΩ and then ground. The report demonstrated that the average output peak has a linear relationship with wind speed. The detection sensitivity of the wind speed was found about 0.09 μA/(m/s). The wind direction can be calculated by analyzing the real-time measured output voltage signals as a mapping image.

Chemical Detection Based Flow Sensor

Wen et al [38], introduced a gas sensor by fabricating a blow-driven triboelectric nanogenerator(BDTENG) via mouth blowing based gas sensor for active alcohol detection. Using a coupling of contact electrification and electrostatic induction, this BDTENG can convert the mechanical energy of air flow to power itself and deliver voltage that has a linear relationship with the breathed-out alcohol concentration in with a sensing range of 10 to 200ppm, regardless of the blowing speed and quality air.

Figure 16 demonstrates the mechanism and structure of the BDTENG. The BDTENG mainly consists of three parts: a stator with Copper electrode, a rotator with FEP & acrylic sheet, and soft elastic. The working principle of the as-developed alcohol sensor can be divided into two aspects. The first one is the air blowing induced electricity generation by coupling between contact electrification, and electrostatic induction, which is the TENG. The later one is the

alcohol adsorption-desorption induced resistance to change, which is the sensor part that is electrically driven by the TENG for gas measurements. Under external pressure, the FEP with the rotator starts rotating and comes in contact with the copper foil on the stator periodically. The charge transfer emerges at the interface due to the potential differences of the two layers and the electron will inject from copper to FEP. During the separation, the generated triboelectric charges remain on the surface due to their lack of mobility. The working mechanism is demonstrated in figure 17.

The gas sensor was tested under different gas blowing speeds mixed with air. The response was recorded by applying a p-type Co_3O_4 external resistive sensor and the result shows that the voltage drop applied over the load by the BDTENG rises along with the load resistance of the sensor. Charge transfer occurs when CO_3O_4 interacts with alcohol which releases free electrons. As a result, the resistance of the sensor rises dramatically, which leads to an increased voltage drop across the sensor and shows a signal to a recorder device, and flashes light as a warning. The response of the BDTENG is shown in figure 18.

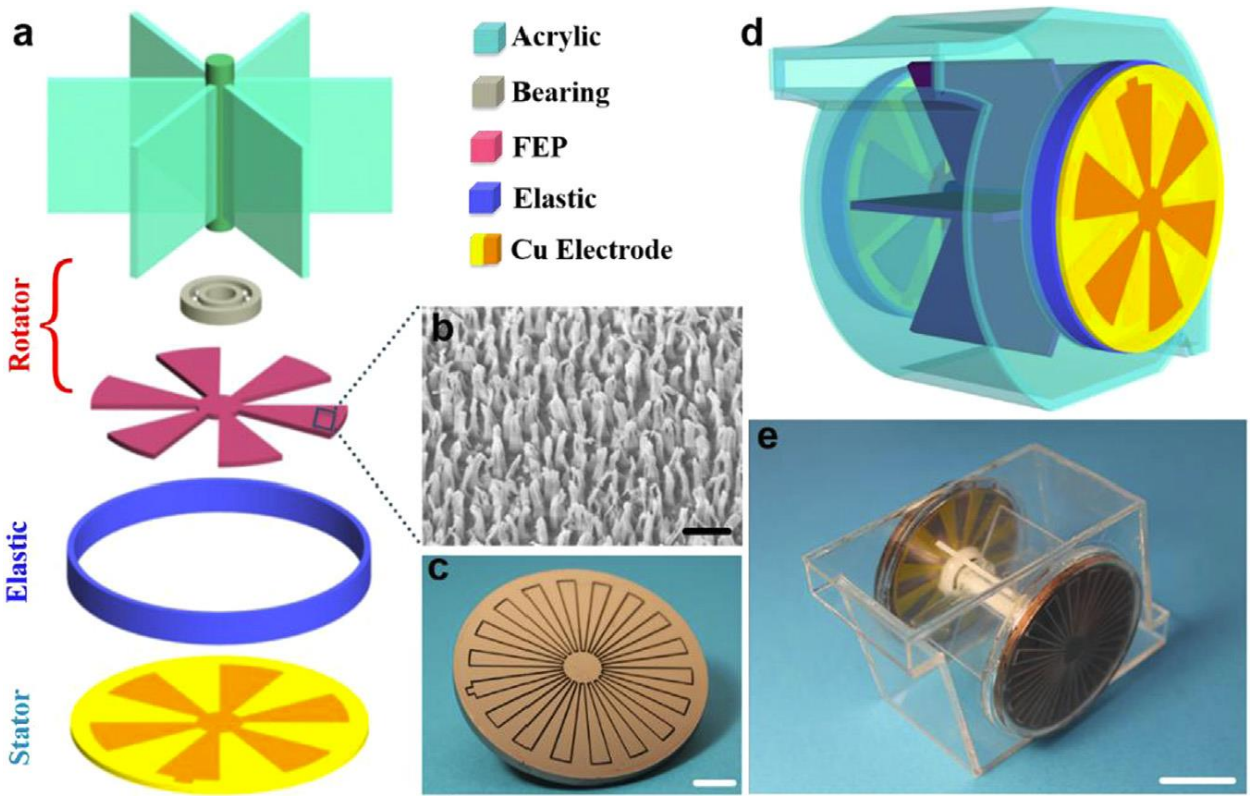

Figure 16: (a) Schematic representations of the functional components of BDTENG.

BDTENG, consists of three parts, a rotator, a stator, and a soft elastic.(b)A SEM image of the

FEP polymer nanowires c)An optical photograph of the as- fabricated stator.(d)A schematic illustration of the BDTENG and(e) a photograph of an as-fabricated BDTENG [38]

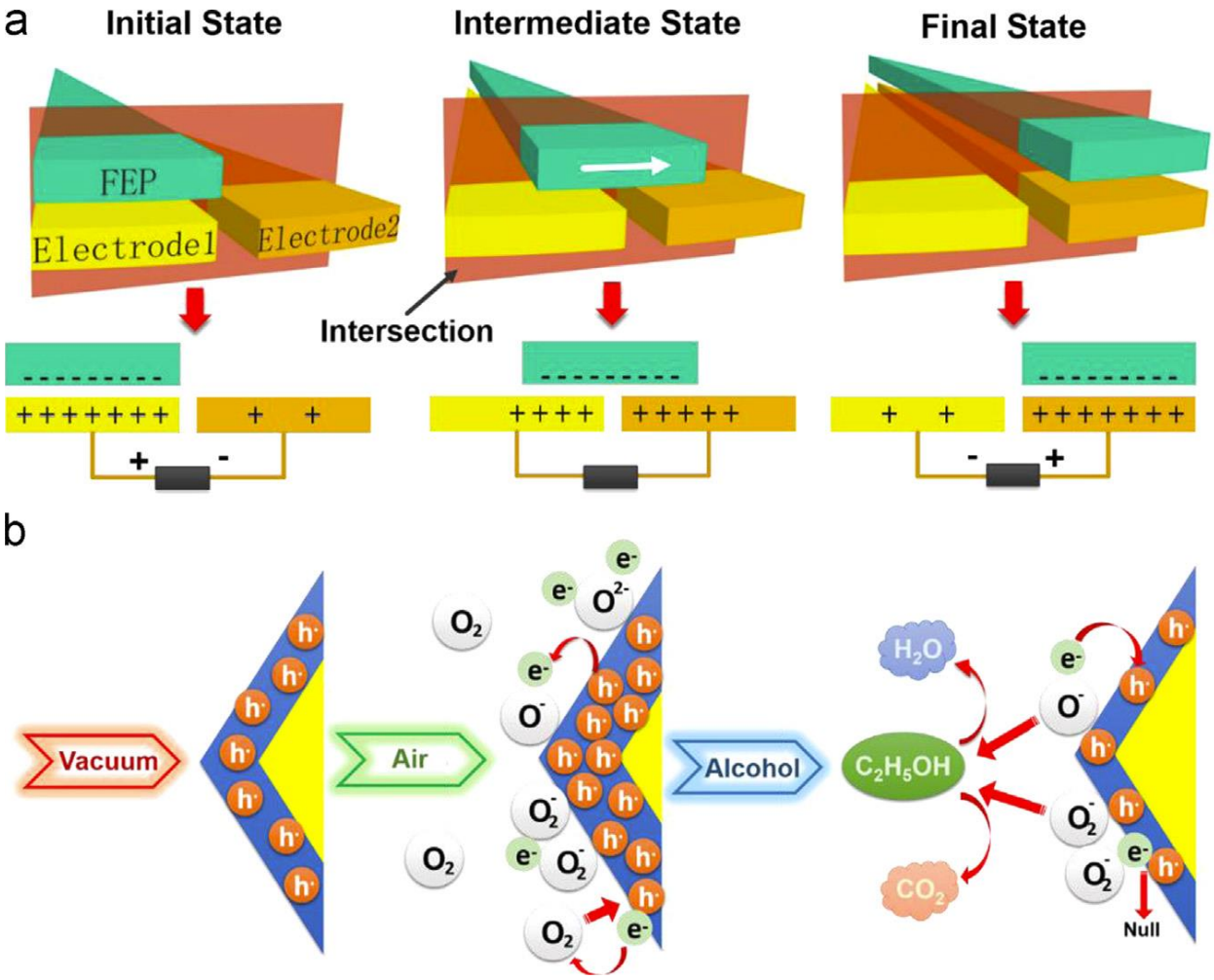

Figure 17: Working mechanism of the BDTENG for self-powered gas sensing. (a)An illustration of the electricity generation process of the BDTENG, which holds three states, the initial state, intermediate state, and final state.(b)Schematic diagram of the chemical reactions under the applied voltage generated by the BDTENG for self- powered gas sensing. And the

proposed chemical reaction process was described as three states, respectively, the surface processes in vacuum, air, and alcohol vapor atmosphere. [38]

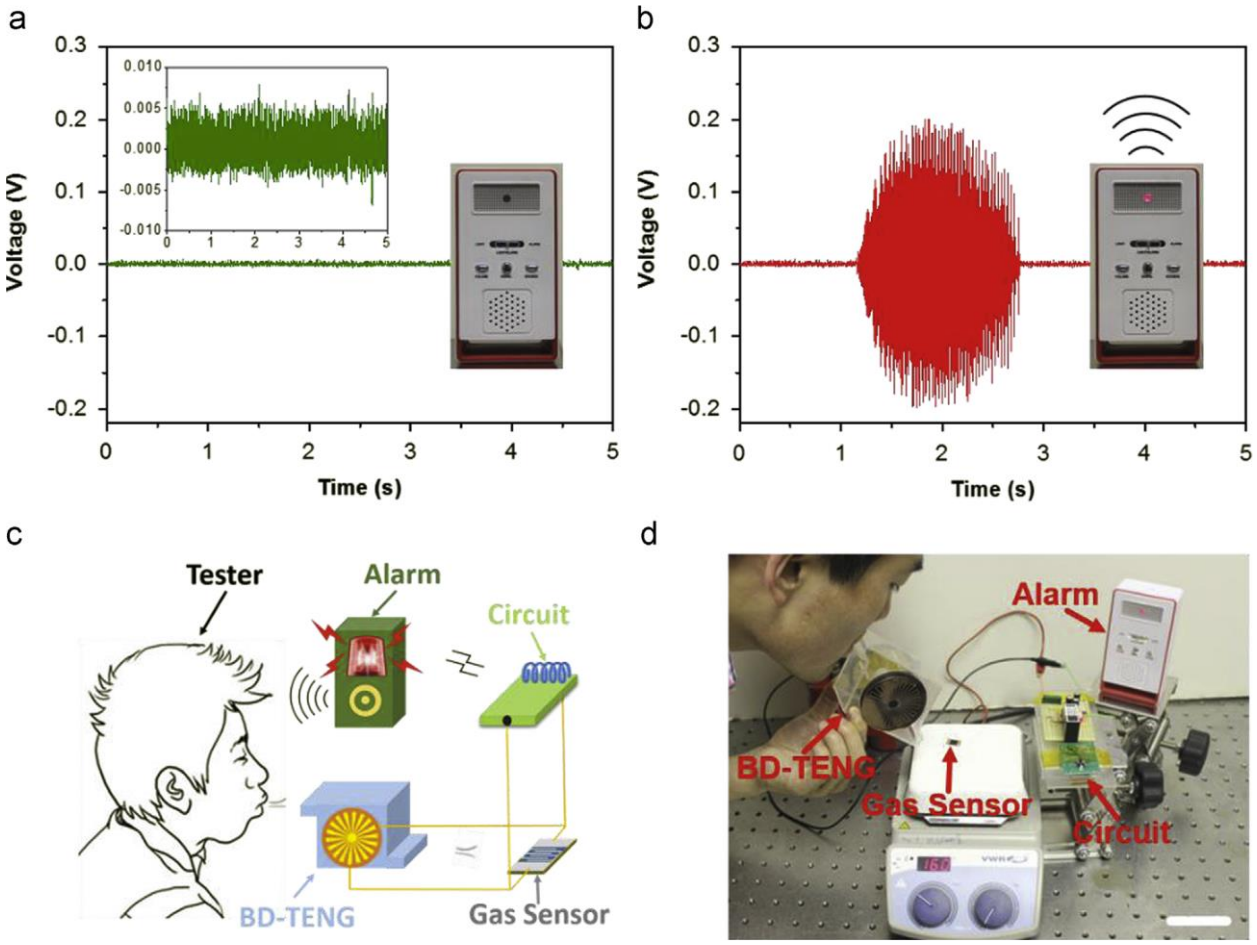

Figure 18: Demonstration of the BDTENG as a self-powered breath analyzer. The acquired voltage output of the BDTENG when it was blown by a tester(a)before and(b)after drinking alcohol. a wireless alarm was triggered with a siren on after drinking alcohol (inset).

(c)A schematic illustration and (d) an optical photograph showing the BDTENG acting as a self-power breath analyzer. The scale bar is 5cm. [38]

Fan et al [47], invented a gas-liquid two-phase flow based on a triboelectric nanogenerator which can work as a self-powered sensor to measure the rising speed of bubbles and converts the kinetic energy of bubbles to electrical energy.

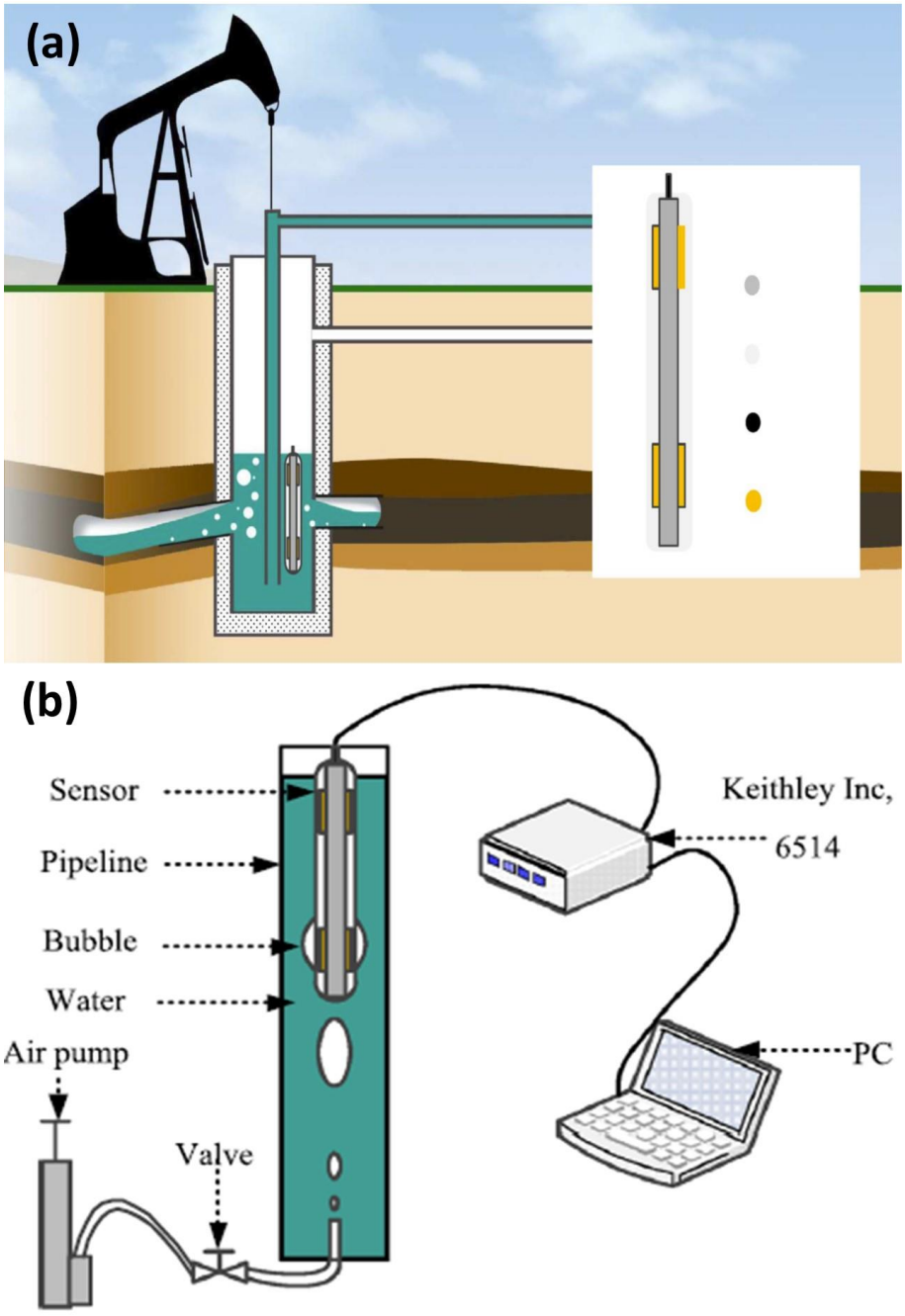

Figure 19: Application environment and structure of GLTTENG, (a) schematic representation of coalbed methane exploitation and GLTTENG installation position, (b) structure and composition of GLTTENG. [47]

The GLTTENG is composed by attaching copper on the upper and lower ends of the acrylic tube and coated the outermost layer with low-density polyethylene (LDPE) to isolate the water and the electrodes (Figure 19a). When the water droplets encounter the GLTTENG the charge transfer starts occurring due to the triboelectric and electrostatic induction effect. When the bubble continues to rise upwards, the charge transfer occurs due to the bubble displacement over the copper electrode of the GLTTENG and generates AC signals (Figure 19b). Two AC current signals will be generated on the top & bottom electrodes for one bubble passing through the GLTTENG. The velocity is measured by dividing this distance by time. This GLTTENG is tested under real-time conditions setting inside a pipeline and creating bubbles from water with the air pump. After conducting 4800 sets of tests and 4 consecutive hours of experiments, it was proved that the measurement accuracy gradually increases with the increase of time intervals between continuous bubbles, and it will reach 100% when the time intervals are greater than 0.3 s while the output voltage remained at about 0.3v with almost no change. The GLTTENG shows that the output voltage rises proportionally with the bubble velocity impulse and the increase of coal dust concentration within the concentration range of 0%–3%, and it also increases gradually with the increase of temperature within the temperature range of 295–360 K, which are all beneficial to improve the signal-to-noise ratio. The largest outputs received from this device are 0.38 V for Voltage, 6.3 nA for current, and 0.64 pW for power with a 50 MΩ external load in series under the condition of bubble velocity impulse of 6200 $cm^3 \cdot cm\ s^{-1}$. This GLTTENG can be used for the potential application of measuring the bubble velocity of gas-liquid two-phase flow in coalbed methane wellbore.

Table 1: Summary of nanogenerator based flow sensors based on their classifications

NG type	Materials	Contact mode	Sub-Division	Voltage	Current	Load	Power	RPM/ Hz	Ref
Bio-medical Application									
TENG	PTFE/Cu	periodic contact/separation		11.1 V	10.2 μA			216 L/min	[52]
TENG	PTFE/Cu	Sliding	Liq	180mV (appx)				1.52 Hz	[51]
			Gas	38mV				1.01 Hz	
TENG	Kapton / Cu/ PTFE	periodic contact/separation			550 μA	400K Ω	25mW	1.5 m/s	[35]
PENG	ZnO nanowires embedded in PDMS layer			61.2 mV	7.12 $nAcm^{-2}$			5.0 ms-1	[34]

Fluid velocity sensing									
PENG	BTZO/PVDF			11.9 V	1.35 μA	11 N	0.2 to 15.8 nW	31.43 to 125.7 m/s	[39]
TENG	FTO glass/ PTFE	Free-standing		38 V	4.2 μA			20 L/min	[53]
STENG	FEP/ Cu	Vertical C/S		36 V	11.8 μA		114.7 μW		[54]
TENG	FEP/Kapton/PTFE/ Cu	freestanding contact mode		6 V	9 μA			9.2 m/s	[42]
TENG	FEP/ Cu	freestanding contact mode			11 μA	100 MΩ	5.9 mW	10 m/s	[48]
EMG-TENG	FEP/Cu	sliding freestanding mode	TENG	48 V		4 MΩ	1.05 mW	500 r min^{-1}	[43]

Hybrid	Cu-Magnets		EMG	4.8 V			58.3 mW		
TENG	FEP/Al	Periodic C/S		100 V	80 μA			10 m/s	[55]
Chemical Detection									
TENG	FEP/Cu	Sliding rotating mode		0.23 V (aprox.)	6 μA (aprox.)	2000 ppm		~	[38]
TENG	Cu/PE	Sliding mode		0.38 V	6.3 nA	50 MΩ	0.64 pW	6200 cm^3.cm s^{-1}	[47]

CHAPTER III

METHODOLOGY AND FINDINGS

Materials and Characterization

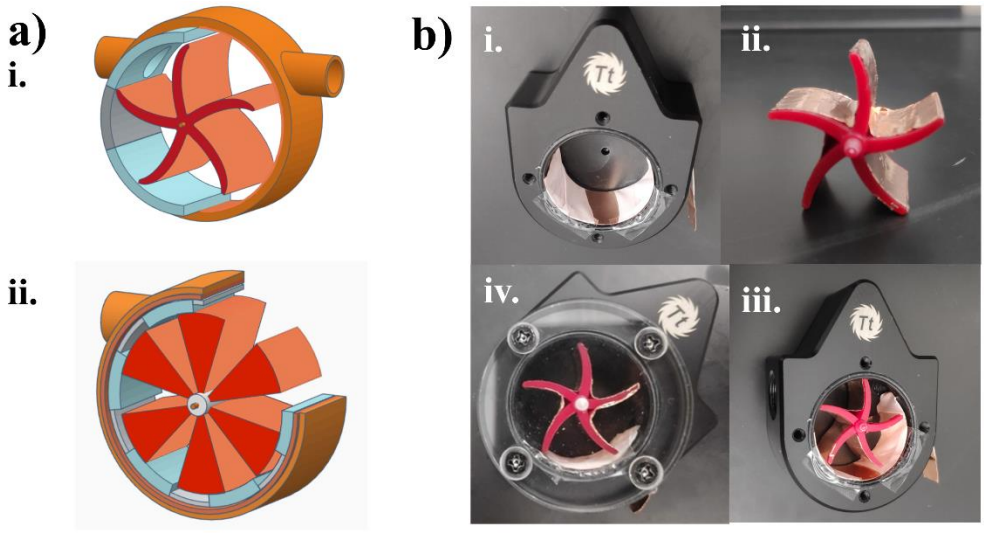

Figure 20: a) Three-dimensional schematic diagram of the Rotating Sliding mode Triboelectric Nanogenerator i) Complete flowmeter, ii) Cross-sectional view of the Internal structure. b) Optical Image of the flowmeter i) The outer part of the Flowmeter, ii) The inner part- impeller, iii) Alignment of the inner & outer part of the TENG, iv) The whole TENG ready to perform

Figure 20 shows the structural design of a Rotating Sliding mode Single electrode Triboelectric Nanogenerator (RS-TENG). The TENG was assembled to work as a flowmeter. This RS-TENG is fabricated by Copper sheet, Teflon tape (Polytetrafluoroethylene-PTFE), Adhesive tape, and Copper tape. In this device, multiphase RS-TENG was made by placing the PTFE tape and adhesive tape side by side layering on the top of the outer copper sheet which is fixed in the wall of the flow indicator (Figure 20 b-i). At the same time, the blades of the device were wrapped by a single layer of copper tape to induce the outer copper sheet electrode. (Figure 20 b-ii). PTFE tape was selected for its outstanding triboelectric charge density (TECD) [56], and copper sheet & tape were chosen because Cu–PTFE makes a very good pair for triboelectrification, especially for the sliding mode TENG [57,58]. Adhesive tape is used for its good insulating. [59] At the same time, copper sheet, Teflon (PTFE) tape, adhesive tape, and copper tape & were preferable for their low thickness (> 0.5 mm) as the impeller won't rotate, if the triboelectric layer becomes even a little thick.

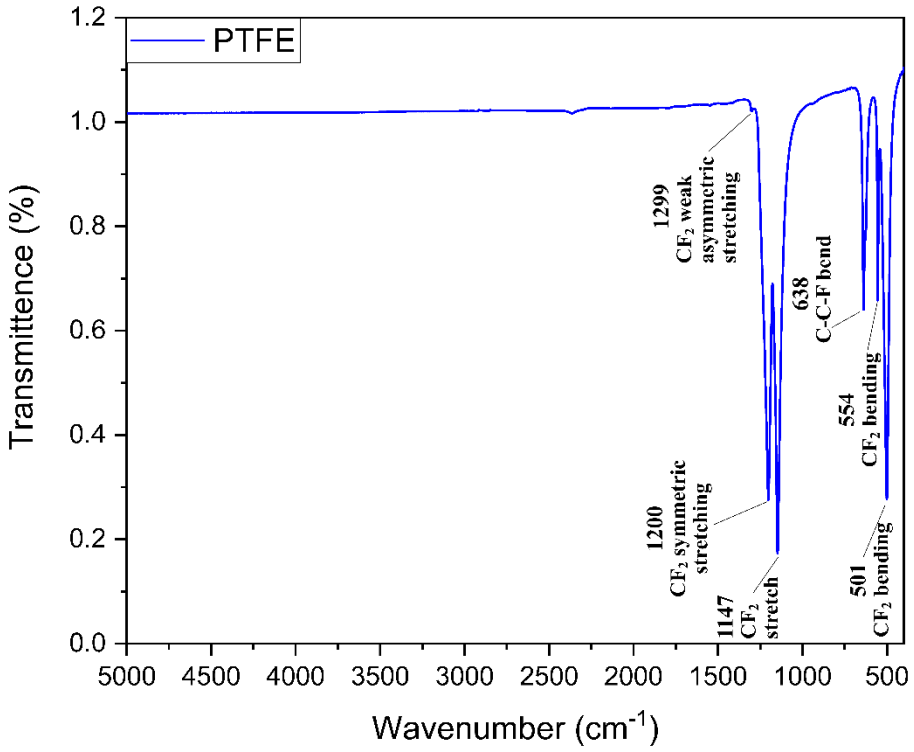

Figure 21: Fourier-transform infrared spectroscopy (FTIR) spectra of the Teflon tape

In this view, Fourier-Transform Infrared (FTIR) spectroscopy analysis was carried out on the Teflon tape, which is made of PTFE ($–[–CF_2 –CF_2–]_n–$). In figure 21, a very weak asymmetric stretching of the CF_2 is visible in the 1299 cm^{-1} region [60], following by one very strong CF_2 symmetric stretching at 1200 cm^{-1} [60,61] and an extremely strong CF_2 stretch at 1147 cm^{-1} [60,61]. However, another peak is notable at the 638 cm^{-1} due to the C-C-F bend [61]. Furthermore, there are two more peaks shown in the 554 cm^{-1} and 501 cm^{-1} region due to a medium CF_2 bending and a strong CF_2 bend respectfully[60]. Compared to already published data and Hitran incorporation, this measured FITR is a well-conforming reference, standard FTIR of PTFE.

Experimental Methods

Fabrication of the TENG

The external structure of this device is a 1.83 x 1.1 x 2.49 inches 5-Blade commercial flow indicator, made of Polyoxymethylene (POM) and Poly(methyl methacrylate) (PMMA). A 1.5-inch x 0.5-inch copper sheet (sigma Aldrich) was wrapped with a single layer 0.6-inch width commercially available PTFE (Teflon) tape for the first 1/3 part. The second 1/3 part of the copper sheet was wrapped with a single layer of 3/4 inch width adhesive tape (Scotch Transparent Tape). The last 1/3 was again wrapped by the same PTFE tape with a single layer. A 0.2-inch x 2-inch copper electrode was attached to the copper sheet to measure the electrical output. The copper sheet along with the PTFE tape & adhesive tape and the copper electrode was fixed inside the device's wall. However, the impellers of the flow indicator were wrapped with a single-layered Copper Foil Tape with Conductive Adhesive(Thermo Fisher Scientific). The copper tape was cut into 0.5-inch x 1 inch to cover each propeller. The copper enfolded impeller was then placed into the flow indicator device, where the tribo-negative layer has been fixed already. Lastly, the transparent plastic layer of the device is placed on the top of the device to prevent any energy loss.

Measuring Output

The output current and voltage were collected with the VersaSTAT3 potentiostat and Tektronix TDS 1001B oscilloscope,[20] while connecting the outer copper electrode connected to the instruments and leaving the other electrode to the ground.

FTIR characterization

Fourier-transform Infrared Spectroscopic analysis was performed using a Perkin Elmer Frontier FTIR Spectrometer. The scan rate was $4s^{-1}$ for the measurement. Relative transmittance was collected in absorbance mode over a full range of wavenumber (4000-450 cm^{-1}).

Working Mechanism

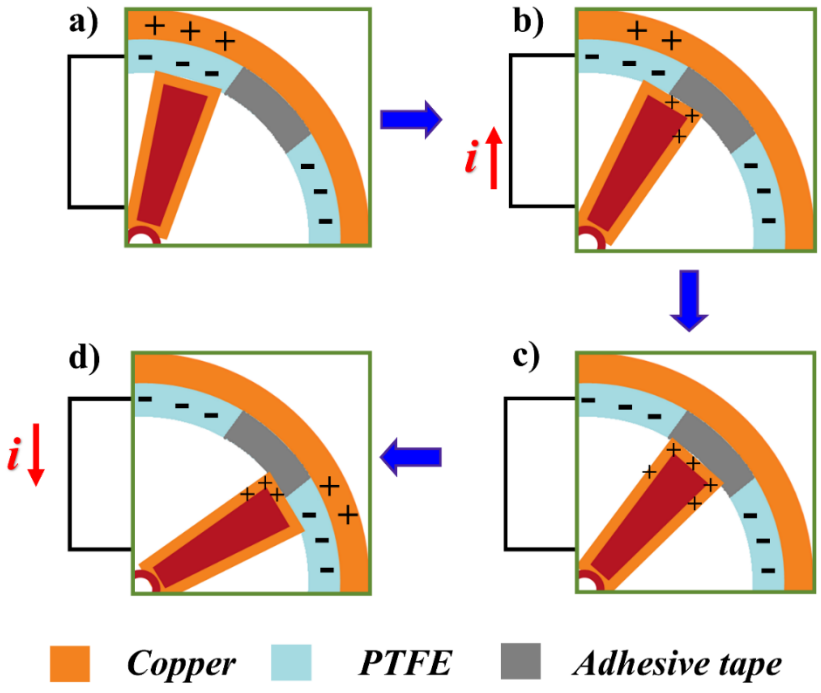

Figure 22: Working principle of the Triboelectric nanogenerator

The working principle of the rotating sliding mode single-electrode triboelectric nanogenerator is discussed in Figure 22. Figure 22a shows the initial stage of the triboelectrification, where the impeller is wrapped by the positive electrode as copper tape touched the tribo-negative PTFE tape attached to the Copper sheet electrode at the top fixed inside the body of the device. As the two sliding contact surfaces come into alignment with each other, the top copper electrode becomes positively charges and the PTFE gets negatively charged due to the contact triboelectrification between the oppositely charged materials. In this stage, the triboelectric charges with opposite polarities are fully balanced out, resulting in no electron transfer.[62] At the second stage (Figure 22b), the impeller starts rotating and the copper-wrapped impeller starts moving forward leaving the PTFE layer and reaches to the adhesive layer. The adhesive tape does not impart any resistance to the movement of the impeller as the adhesive layer stays on the opposite side (towards copper tape) of the impeller. Due to the sliding, the polarization balance gets disturbed and this mismatch leads to a voltage difference. To neutralize the polarizing effect, the electron starts moving from the top Copper sheet electrode to the bottom copper-wrapped sliding impeller through the external circuit.[57] The electron keeps flowing in the same direction till the impeller reached the adhesive tape completely where positive copper-wrapped impeller and negative PTFE come in full separation and the positive triboelectric charges are fully transferred from the top copper sheet to the bottom copper tape. (Figure 22c). As the impeller rotates, the impeller comes into another PTFE layer and the electron starts flowing back in an opposite direction to balance (22d) and obtain the initial position (22a) resulting an AC signal in the output.

Investigation of Sensory Application

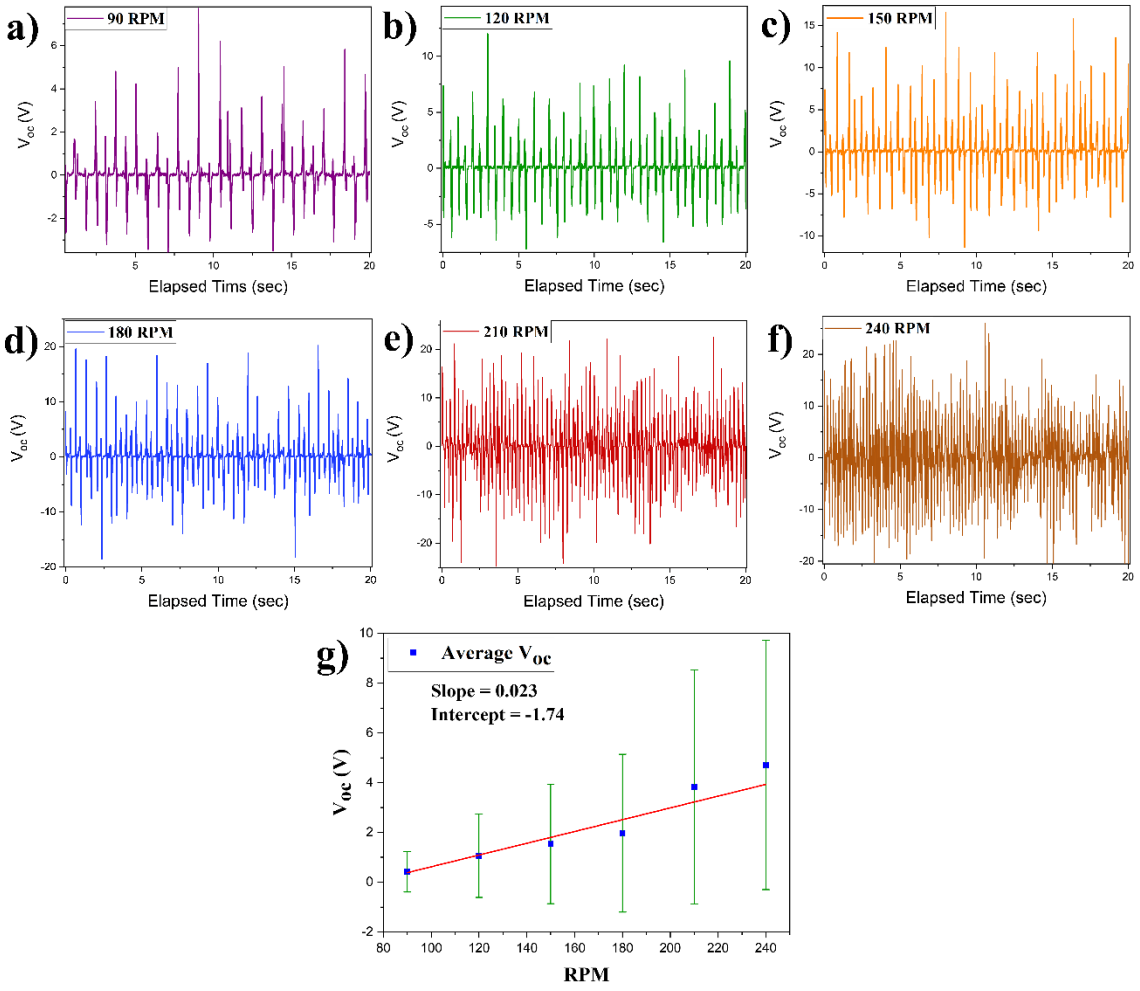

Figure 23: Performance of rotating sliding mode TENG at a) 90, b) 120, c) 150, d) 180, e) 210, f) 240 RPM for Open Circuit Voltage g) Calibration curve for the V_{oc} for different RPM along with the error bar

To check the feasibility of the TENG, a nanogenerator unit was made of 1.5inch x 0.5inch in size for the upper electrode and lower electrode, and the multiphase was created by putting the PTFE and adhesive layers side by side. When the copper tape starts sliding over the PTFE coated top copper layer, triboelectric potential generates and gets transmitted to the copper layered impeller. The impeller surface shows a repulsive force to prevent itself from getting induced. As a result, the overall open circuit voltage reduces a little. But the rotating chamber forces the impeller to get deflected and increases the voltage to achieve its peak. Then the impeller rotates to travel through the adhesive layer and the next PTFE layer showing a slow response due to micro relaxation and micro stresses by the impact of round shaped impact creating device. When the impeller moves back to another PTFE layer, the charges start flowing in the opposite direction showing a gradual decrease in the output voltage. [11,20] Then the open circuit voltage was measured in various RPM. In figure 23, the maximum open-circuit voltages obtained are 7.72 V, 12.02 V, 11.8 V, 20.2 V, 22.6 V, 26 V from the 90 RPM, 120 RPM, 150 RPM, 180 RPM, 210 RPM, and 240 RPM, respectively. Due to the inconsistency of force during sliding motion, the output voltage and current showed inconsistent behavior. [11,63] In figure 23g, a calibration curve is drawn for the open-circuit voltage on the basis of getting the minimum standard deviation for each RPM. In this graph, the slope is 0.023 and the y-axes intercept is -1.74. From this curve, it can be clearly seen that the output response is much better in the higher frequency. As a result, the electrons in the external circuit gets shorter time to neutralize the triboelectric potential leading towards a larger flow of electron.[64] The average shows the responses are close for lower and mid RPMs comparing to the higher RPMs.

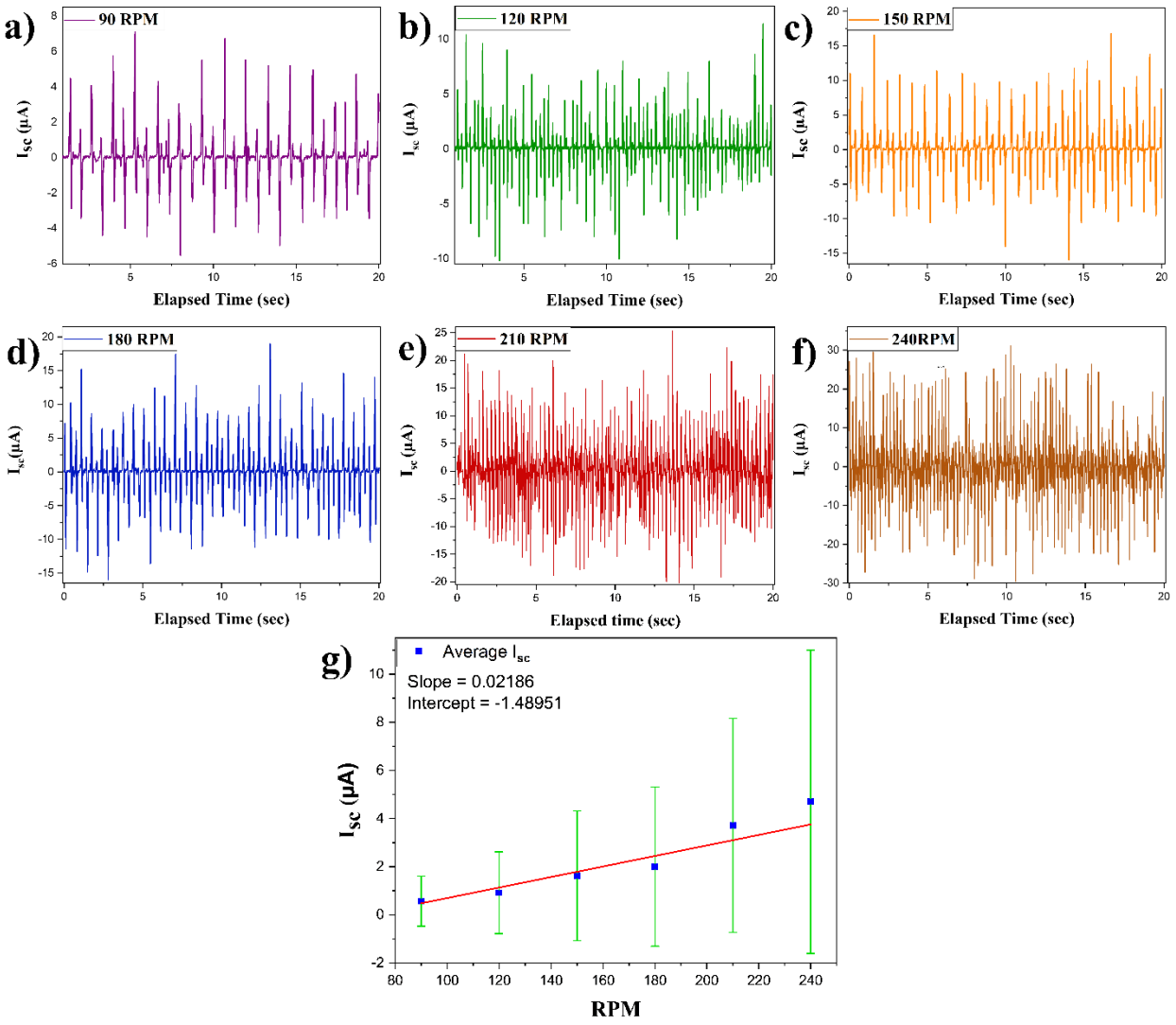

Figure 24: Performance of rotating sliding mode TENG at a) 90, b) 120, c) 150, d) 180, e) 210, f) 240 RPM for Short Circuit Current g) Calibration curve for the I_{sc} for different RPM with the error bar

To continue the feasibility test for the short circuit current, the as-made TENG unit was used further. The maximum output current observed for the single unit was 7.12, 10.4, 16.8, 19, 25.3, and 31.2 µA

(Fig. 24) for 90, 120, 150, 180, 210 and 240 RPM load frequencies respectively. The output performance rises parallelly with the increment of the load frequency. The calibration curve in figure 5 made it clear that the average value of lower frequencies, such as 90, 120, 150, 180 increases gradually. But in turns of higher frequency like 210 & 240, the average value catches a sharp increase. This happened due to the increase in the number of contacts as the electron doesn't get enough time to get back to its original position and neutralize the circuit. As a result, higher output is observed in greater load.

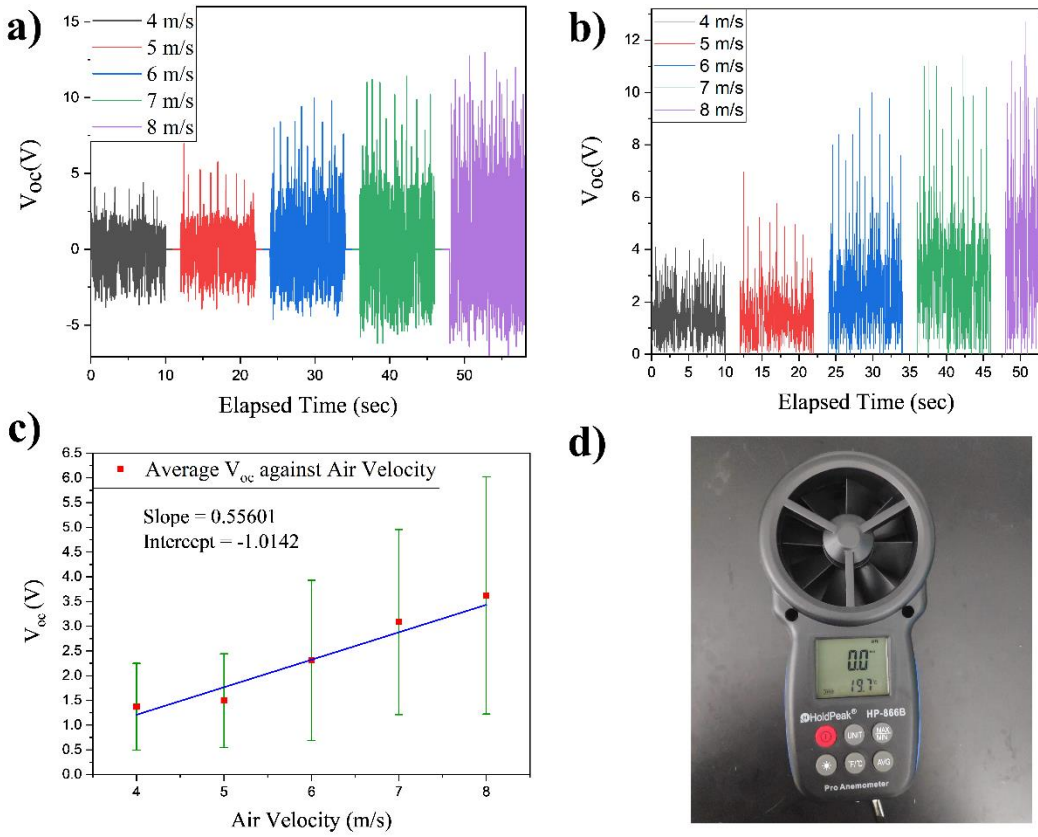

Figure 25: Performance of the flow meter for Open Circuit Voltage with an anemometer a) with air velocity of 4m/s, 5m/s, 6m/s, 7m/s, and 8m/s. b) absolute value of the of 4m/s, 5m/s, 6m/s, 7m/s and 8m/s. c) The calibration curve with the error bars d) optical image of the anemometer

To characterize the electrical output, V_{oc} of the rotating sliding mode single electrode TENG was tested at various air velocities (Figure 25). For the 4 m/s air velocity, the maximum open-circuit voltage 4.4 V, whereas the average output is shown as 1.37 V. On the other hand, the 5 m/s air speed produces the maximum potential of 6.96 V, though the average is 1.5 V, which is very close to the previous velocity. 10 V is the highest performance shown by the 6 m/s air rate, however, the average is still as low as 2.3 V. When the air velocity is increased and put into 7 m/s & 8 m/s, the peaks do not go that high and remains as 11.4 V and 12.98 V, respectively. But they show constant performance in comparison to the other lower speed outputs. As a result, the average value increases and reaches up to 3.08 V & 3.62V, respectfully.

These phenomena can be explained by the kinetic energy increasing hugely with the multiplication of growing velocity by itself. When the air velocity was lower, the electrical energy was going high with the rate of kinetic energy produced by the air speed. When the air velocity gets higher, the copper electrodes get saturated by the charges generating from the rotating motion created by the kinetic energy. At that point, the peaks get denser than the lower speeds peak. This is the reason the maximum power output cannot rise sharply, rather than the average value gets high with the greater velocity. The absolute values from figure 6b help to understand this process better.

The calibration curve for the average open circuit voltage against the air velocity is shown in figure 6c. The error bar is counted by the standard deviation and the straight line is drawn to make it best fitted to minimize the standard deviation. For the air speed of 4, 5, 6, 7 & 8 m/s the error bar is 0.88, 0.95, 1.62, 1.87 and 2.4, respectively. This graph can be used to determine the unknown air velocity as well as work as a flowmeter chart.

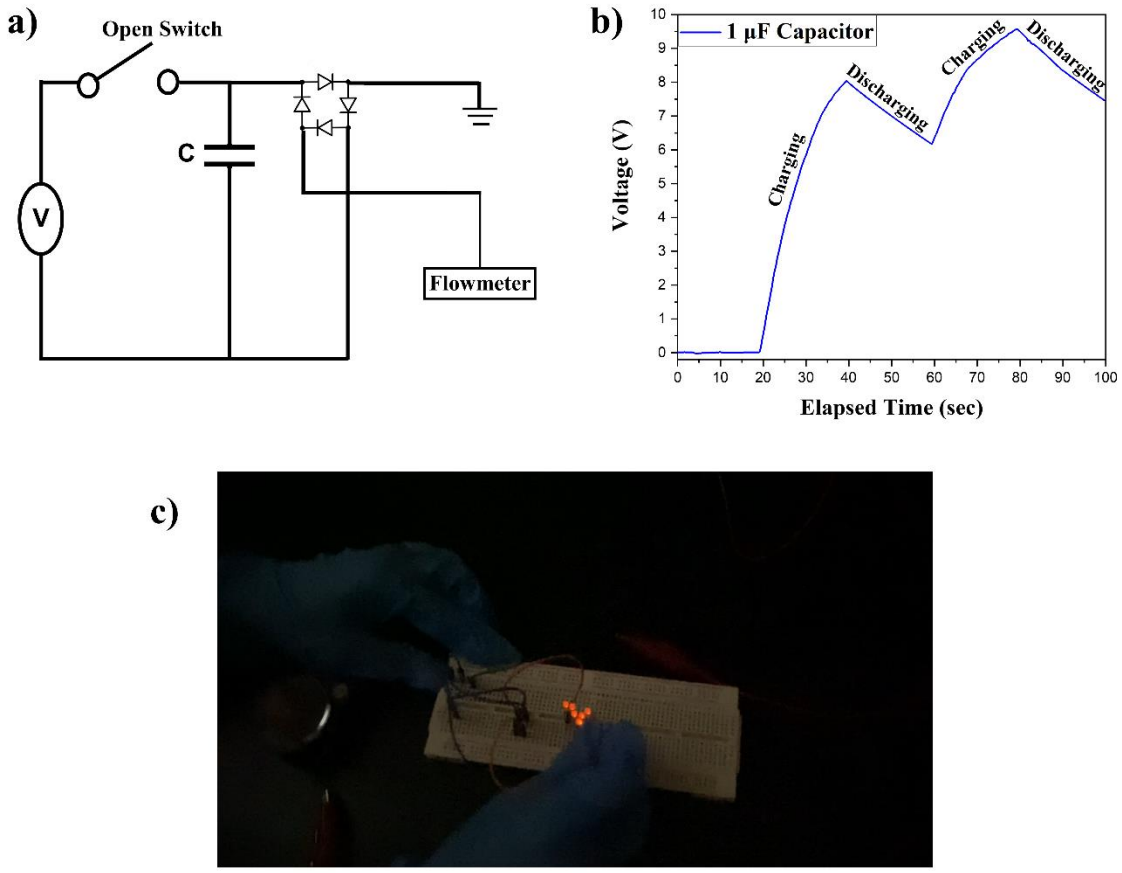

Figure 26: (a) Circuit Diagram to run the capacitor test with the flow sensor. (b) Charging and discharging of 1µF capacitor with the flowmeter (c) Lighting 7 LEDs with the flowmeter

Figure 26 (a) shows the circuit diagram to conduct the capacitor and LED lightening test. Here, a 1µF ceramic capacitor was parallelly connected to the bridge rectifier and the flow sensor. As the single-electrode triboelectric nanogenerator was used in this device, the other part of the input wire was connected to the ground to complete the circuit. Figure 26(b) shows the charging and discharging ability of the flowmeter with an interval of 20 seconds each. This data was taken at a constant air velocity of 6 m/s and the 1µF capacitor reached the highest energy storage potential from this test was 9.57 V. After getting stabilized for 20 seconds from the initial

time, the potential has a sharp rise in the first 20 seconds and went up to 8.03 V. Then the capacitor started releasing energy for 20 seconds and falls into 6.17 V. The capacitor was again charged from time interval of 60 seconds to 80 seconds. In this phase, the highest value was observed, and the potential reached 9.57 V. The released charge of the capacitor reached 7.47 V for the last 20 seconds. As the charges were accumulated during charging operation continuously, it took more time to discharge after reaching a higher voltage than the first cycle. These two cycles of 100 seconds prove that the flowmeter is capable of using as a self-powered device by connecting a simple power storage battery.

The flowmeter was further tested by lightening Light Emitting Diodes (LEDs)s for practical demonstration (Figure 26(c)). For this experiment, the same circuit was used as the capacitor test. 7 LEDs were connected in series and parallelly with the 1µF capacitor, bridge rectifier, and flow sensor. This circuit was controlled by a switch. At the initial stage the switch remains off, and the capacitor was charged at a constant air speed of 6 m/s. The switch was closed after energy storage accumulated in the capacitor, resultant in fully light up 7 LEDs. The supplementary video(S1) shows the real-time energy powering which leads to the potential of a self-powered flow sensor. The calibration curve shows the average open circuit voltage with respect to the air velocity.

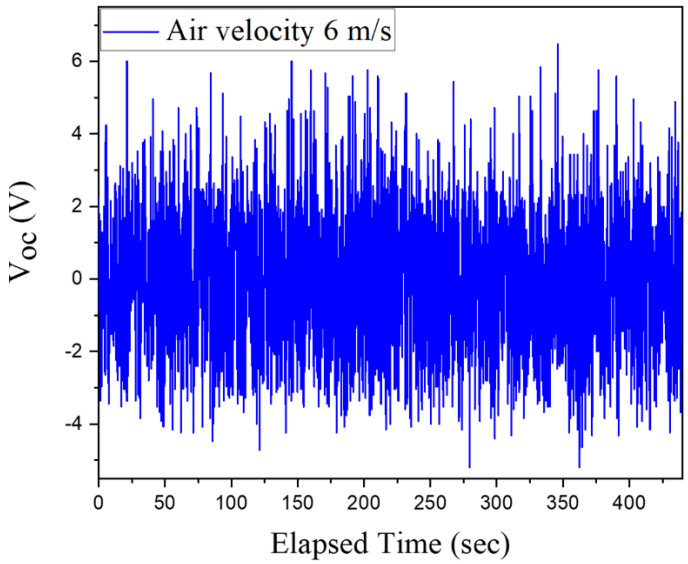

Figure 27: Robustness and stability investigation of the RS-TENG. No obvious electrical output decay was observed after 460 sec (at a fixed air velocity of 6m/s).

The RS-TENG was furthered explored with continuous application of cycled air velocity of 6 m/s. Notably, there were no significant differences in the output voltages and no significant distortion or serious damage after continuous measuring from the flow sensor over 460 seconds (Figure 27). This confirms the excellent mechanical durability of our RS-TENG in this work. Also, a very little amount of electrical output fluctuation was observed. The outstanding robustness enables long-term stability, which is considered an important improvement of this RS-TENG as a flow sensor.

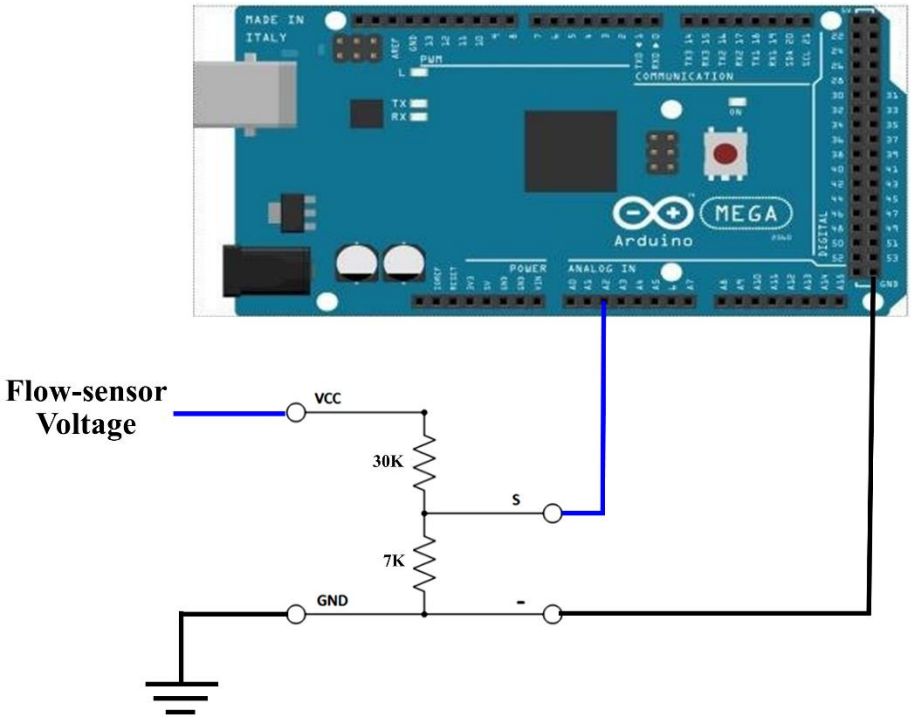

Figure 28: Circuit diagram for Arduino 2560 Mega board

Figure 28 illustrates a circuit diagram to connect the flow sensor to the Arduino board to read the voltage on the display screen. For the Arduino mega 2560 board, the loop reads the analog value from the analog input, and because the reference voltage is 5 V, it multiples that value by 5, then divides by 2048 to get the actual value.[65] In order to measure voltages greater than the 5 V reference voltage, a voltage sensor was used for the input voltage so that the voltage actually input to the Arduino is 5 V or less. in this experiment, a 30k ohm resistor and a 7k ohm resistor were used to create a 30:7 divider. This will allow us to measure voltages up to 21.4 V to calculate the actual voltage value. [65] To complete the circuit, the "S" and "–" pins (figure 9) of the Voltage Sensor were connected to A2 (Analog Input) and GND of Arduino respectively. Then the external voltage pins (VCC & GND) were connected to the flow sensor to measure the voltage.[66] The real-life velocity measurement by calibrating the input voltage using an

Arduino board was shown in the supporting video.(S3) Here, also the velocity is showing 1, 3 & 6 m/s for the air velocity of 6 m/s. These phenomena were explained in figure 3 by the charge accumulation theory of the triboelectric nanogenerator. As the charge density reaches its peak after reaching the highest output, the RS-TENG starts to release the accumulated charges, so that it can gradually increase the output potential again.

Conclusion

In summary, a simple, cost-effective, yet energy harvesting rotating sliding mode triboelectric nanogenerator (RS-TENG) flow sensor was developed to convert the kinetic energy of the air velocity to electrical energy, as well as to measure the air flowrate. This flowmeter is composed of copper sheets, PTFE tape, adhesive tape, and copper tape. To check the feasibility, a separate single unit of TENG was tested under variable RPMs to measure the electrical performance. Based on this information two separate calibration curve was prepared for the open-circuit voltage and short circuit current, respectfully. Moreover, the flow sensor was further tested under the real-life condition with the air velocity of 4, 5, 6, 7, and 8 m/s and the highest open-circuit voltage observed in respect to the previous velocity's are, 4.4 V, 6.96 V, 10 V, 11.4 V, and 12.98 V, respectively. This flowmeter was further tested with 1 μF capacitor and able to light up 7 LEDs which implies this device can work as a self-powered flow sensor opening a new area in large-scale industrial use.

REFERENCES

[1] S. Vaidya, P. Ambad, S. Bhosle, Industry 4.0 – A Glimpse, Procedia Manufacturing. 20 (2018) 233–238. https://doi.org/10.1016/j.promfg.2018.02.034.

[2] E.N. Jacobs, K.E. Ward, R.M. Pinkerton, The characteristics of 78 related airfoil sections from tests in the variable-density wind tunnel, UNT Digital Library. (1932). https://digital.library.unt.edu/ark:/67531/metadc65698/ (accessed January 11, 2021).

[3] E. Islam, A.M. Abdullah, A.R. Chowdhury, F. Tasnim, M. Martinez, C. Olivares, K. Lozano, M.J. Uddin, Electromagnetic-triboelectric-hybrid energy tile for biomechanical green energy harvesting, Nano Energy. 77 (2020) 105250. https://doi.org/10.1016/j.nanoen.2020.105250.

[4] R.W. Miller, Flow measurement engineering handbook, (1983). https://www.osti.gov/biblio/6037678-flow-measurement-engineering-handbook (accessed January 11, 2021).

[5] Decentralized triboelectric electronic health monitoring flexible microdevice - Chowdhury - 2020 - MEDICAL DEVICES & SENSORS - Wiley Online Library, (n.d.). https://onlinelibrary.wiley.com/doi/full/10.1002/mds3.10103 (accessed March 2, 2021).

[6] A.R. Chowdhury, J. Jaksik, I. Hussain, P. Tran, S. Danti, M.J. Uddin, Surface-Modified Nanostructured Piezoelectric Device as a Cost-Effective Transducer for Energy and Biomedicine, Energy Technology. 7 (2019) 1800767. https://doi.org/10.1002/ente.201800767.

[7] A.R. Chowdhury, J. Jaksik, I. Hussain, R. Longoria, O. Faruque, F. Cesano, D. Scarano, J. Parsons, M.J. Uddin, Multicomponent nanostructured materials and interfaces for efficient piezoelectricity, Nano-Structures & Nano-Objects. 17 (2019) 148–184. https://doi.org/10.1016/j.nanoso.2018.12.002.

[8] S. Rajala, T. Siponkoski, E. Sarlin, M. Mettänen, M. Vuoriluoto, A. Pammo, J. Juuti, O.J. Rojas, S. Franssila, S. Tuukkanen, Cellulose Nanofibril Film as a Piezoelectric Sensor Material, ACS Appl. Mater. Interfaces. 8 (2016) 15607–15614. https://doi.org/10.1021/acsami.6b03597.

[9] C.M. Bruinink, R.K. Jaganatharaja, M.J. de Boer, E. Berenschot, M.L. Kolster, T.S.J. Lammerink, R.J. Wiegerink, G.J.M. Krijnen, Advancements in Technology and Design of Biomimetic Flow-Sensor Arrays, in: 2009 IEEE 22nd International Conference on Micro Electro Mechanical Systems, 2009: pp. 152–155. https://doi.org/10.1109/MEMSYS.2009.4805341.

[10] Z.L. Wang, J. Song, Piezoelectric Nanogenerators Based on Zinc Oxide Nanowire Arrays, Science. 312 (2006) 242–246. https://doi.org/10.1126/science.1124005.

[11] Lithium doped zinc oxide based flexible piezoelectric-triboelectric hybrid nanogenerator - ScienceDirect, (n.d.). https://www.sciencedirect.com/science/article/abs/pii/S2211285519303866 (accessed May 8, 2020).

[12] Z.L. Wang, Toward self-powered sensor networks, Nano Today. 5 (2010) 512–514. https://doi.org/10.1016/j.nantod.2010.09.001.

[13] D.B. Deutz, N.T. Mascarenhas, J.B.J. Schelen, D.M. de Leeuw, S. van der Zwaag, P. Groen, Flexible Piezoelectric Touch Sensor by Alignment of Lead-Free Alkaline Niobate Microcubes in PDMS, Advanced Functional Materials. 27 (2017) 1700728. https://doi.org/10.1002/adfm.201700728.

[14] X. Gao, M. Zheng, X. Yan, J. Fu, M. Zhu, Y. Hou, The alignment of BCZT particles in PDMS boosts the sensitivity and cycling reliability of a flexible piezoelectric touch sensor, J. Mater. Chem. C. 7 (2019) 961–967. https://doi.org/10.1039/C8TC04741C.

[15] C.-C. Chen, T.-K. Chung, C.-Y. Tseng, C.-F. Hung, P.-C. Yeh, C.-C. Cheng, A Miniature Magnetic-Piezoelectric Thermal Energy Harvester, IEEE Transactions on Magnetics. 51 (2015) 1–9. https://doi.org/10.1109/TMAG.2015.2395385.

[16] Y.K. Fetisov, A.A. Bush, K.E. Kamentsev, A.Y. Ostashchenko, G. Srinivasan, Ferrite-Piezoelectric Multilayers for Magnetic Field Sensors, IEEE Sensors Journal. 6 (2006) 935–938. https://doi.org/10.1109/JSEN.2006.877989.

[17] W.Patrick. Carey, B.R. Kowalski, Chemical piezoelectric sensor and sensor array characterization, Anal. Chem. 58 (1986) 3077–3084. https://doi.org/10.1021/ac00127a037.

[18] W. Pang, H. Zhao, E. Sok Kim, H. Zhang, H. Yu, X. Hu, Piezoelectric microelectromechanical resonant sensors for chemical and biological detection, Lab on a Chip. 12 (2012) 29–44. https://doi.org/10.1039/C1LC20492K.

[19] Wireless sensor node with hybrid energy harvesting for air-flow rate sensing - IEEE Conference Publication, (n.d.). https://ieeexplore.ieee.org/document/8234161 (accessed February 23, 2021).

[20] Organic-Inorganic Hybrid Materials for Piezoelectric/Triboelectric Nanogenerator - ProQuest, (n.d.). https://search.proquest.com/openview/a47c506d20c98e8e9bbd4586b7f37bce/1?pq-origsite=gscholar&cbl=18750&diss=y (accessed January 13, 2020).

[21] F.-R. Fan, Z.-Q. Tian, Z. Lin Wang, Flexible triboelectric generator, Nano Energy. 1 (2012) 328–334. https://doi.org/10.1016/j.nanoen.2012.01.004.

[22] F. Tasnim, S.A. Iqbal, A.R. Chowdhury, Biogas production from anaerobic co-digestion of cow manure with kitchen waste and Water Hyacinth, Renewable Energy. 109 (2017) 434–439. https://doi.org/10.1016/j.renene.2017.03.044.

[23] S.A. Iqbal, F. Tasnim, A.R. Chowdhury, A. Islam, T. Islam, MUNICIPAL SOLID WASTE MANAGEMENT IN SYLHET CITY CORPORATION, (n.d.) 7.

[24] J. Lowell, A.C. Rose-Innes, Contact electrification, Advances in Physics. 29 (1980) 947–1023. https://doi.org/10.1080/00018738000101466.

[25] K.A. Sharp, B. Honig, Electrostatic Interactions in Macromolecules: Theory and Applications, Annual Review of Biophysics and Biophysical Chemistry. 19 (1990) 301–332. https://doi.org/10.1146/annurev.bb.19.060190.001505.

[26] Air-Flow-Driven Triboelectric Nanogenerators for Self-Powered Real-Time Respiratory Monitoring | ACS Nano, (n.d.). https://pubs.acs.org/doi/10.1021/acsnano.8b02562 (accessed April 26, 2020).

[27] L.A. Weinstein, M.R. Cacan, P.M. So, P.K. Wright, Vortex shedding induced energy harvesting from piezoelectric materials in heating, ventilation and air conditioning flows, Smart Mater. Struct. 21 (2012) 045003. https://doi.org/10.1088/0964-1726/21/4/045003.

[28] Self-powered wireless sensor node for flow and temperature sensing - IOPscience, (n.d.). https://iopscience.iop.org/article/10.1088/1742-6596/1052/1/012092 (accessed February 24, 2021).

[29] P. Skládal, C. dos S. Riccardi, H. Yamanaka, P.I. da Costa, Piezoelectric biosensors for real-time monitoring of hybridization and detection of hepatitis C virus, Journal of Virological Methods. 117 (2004) 145–151. https://doi.org/10.1016/j.jviromet.2004.01.005.

[30] P. Wang, S. Zhang, L. Zhang, L. Wang, H. Xue, Z.L. Wang, Non-contact and liquid–liquid interfacing triboelectric nanogenerator for self-powered water/liquid level sensing, Nano Energy. 72 (2020) 104703. https://doi.org/10.1016/j.nanoen.2020.104703.

[31] H. Zhong, J. Xia, F. Wang, H. Chen, H. Wu, S. Lin, Graphene-Piezoelectric Material Heterostructure for Harvesting Energy from Water Flow, Advanced Functional Materials. 27 (2017) 1604226. https://doi.org/10.1002/adfm.201604226.

[32] D. Zheng, T. Zhang, Y. Hu, Experimental investigations of the location of a piezoelectric probe in a vortex flow sensor, Meas. Sci. Technol. 18 (2007) 3777–3783. https://doi.org/10.1088/0957-0233/18/12/012.

[33] H. Zhang, Y. Yang, Y. Su, J. Chen, C. Hu, Z. Wu, Y. Liu, C. Ping Wong, Y. Bando, Z.L. Wang, Triboelectric nanogenerator as self-powered active sensors for detecting

liquid/gaseous water/ethanol, Nano Energy. 2 (2013) 693–701. https://doi.org/10.1016/j.nanoen.2013.08.004.

[34] H.-I. Lin, R.-H. Horng, D.-S. Wuu, ZnO Nanogenerator as a Wind Speed Sensor for Human Respiration Detector, Meet. Abstr. MA2013-01 (2013) 1492. https://doi.org/10.1149/MA2013-01/45/1492.

[35] S. Wang, X. Mu, X. Wang, A.Y. Gu, Z.L. Wang, Y. Yang, Elasto-Aerodynamics-Driven Triboelectric Nanogenerator for Scavenging Air-Flow Energy, ACS Nano. 9 (2015) 9554–9563. https://doi.org/10.1021/acsnano.5b04396.

[36] Y. Yang, G. Zhu, H. Zhang, J. Chen, X. Zhong, Z.-H. Lin, Y. Su, P. Bai, X. Wen, Z.L. Wang, Triboelectric Nanogenerator for Harvesting Wind Energy and as Self-Powered Wind Vector Sensor System, ACS Nano. 7 (2013) 9461–9468. https://doi.org/10.1021/nn4043157.

[37] Airflow-Induced Triboelectric Nanogenerator as a Self-Powered Sensor for Detecting Humidity and Airflow Rate | ACS Applied Materials & Interfaces, (n.d.). https://pubs.acs.org/doi/10.1021/am504919w (accessed February 25, 2021).

[38] Z. Wen, J. Chen, M.-H. Yeh, H. Guo, Z. Li, X. Fan, T. Zhang, L. Zhu, Z.L. Wang, Blow-driven triboelectric nanogenerator as an active alcohol breath analyzer, Nano Energy. 16 (2015) 38–46. https://doi.org/10.1016/j.nanoen.2015.06.006.

[39] N.R. Alluri, B. Saravanakumar, S.-J. Kim, Flexible, Hybrid Piezoelectric Film (BaTi(1–x)ZrxO3)/PVDF Nanogenerator as a Self-Powered Fluid Velocity Sensor, ACS Appl. Mater. Interfaces. 7 (2015) 9831–9840. https://doi.org/10.1021/acsami.5b01760.

[40] Self-Powered Triboelectric Micro Liquid/Gas Flow Sensor for Microfluidics | ACS Nano, (n.d.). https://pubs.acs.org/doi/10.1021/acsnano.6b04440 (accessed February 25, 2021).

[41] Segmented wind energy harvester based on contact-electrification and as a self-powered flow rate sensor - ScienceDirect, (n.d.). https://www.sciencedirect.com/science/article/abs/pii/S0009261416302652?via%3Dihub (accessed February 25, 2021).

[42] M. Xu, Y.-C. Wang, S.L. Zhang, W. Ding, J. Cheng, X. He, P. Zhang, Z. Wang, X. Pan, Z.L. Wang, An aeroelastic flutter based triboelectric nanogenerator as a self-powered active wind speed sensor in harsh environment, Extreme Mechanics Letters. 15 (2017) 122–129. https://doi.org/10.1016/j.eml.2017.07.005.

[43] Y. Zhong, H. Zhao, Y. Guo, P. Rui, S. Shi, W. Zhang, Y. Liao, P. Wang, Z.L. Wang, An Easily Assembled Electromagnetic-Triboelectric Hybrid Nanogenerator Driven by Magnetic Coupling for Fluid Energy Harvesting and Self-Powered Flow Monitoring in a Smart Home/City, Advanced Materials Technologies. 4 (2019) 1900741. https://doi.org/10.1002/admt.201900741.

[44] Q. Zeng, Y. Wu, Q. Tang, W. Liu, J. Wu, Y. Zhang, G. Yin, H. Yang, S. Yuan, D. Tan, C. Hu, X. Wang, A high-efficient breeze energy harvester utilizing a full-packaged triboelectric nanogenerator based on flow-induced vibration, Nano Energy. 70 (2020) 104524. https://doi.org/10.1016/j.nanoen.2020.104524.

[45] T.K. Phan, S. Wang, Y. Wang, H. Wang, X. Xiao, X. Pan, M. Xu, J. Mi, A Self-Powered and Low Pressure Loss Gas Flowmeter Based on Fluid-Elastic Flutter Driven Triboelectric Nanogenerator, Sensors. 20 (2020) 729. https://doi.org/10.3390/s20030729.

[46] P. Cheng, M. Sun, C. Zhang, H. Guo, J. Shi, Y. Zhang, Y. Liu, J. Wang, Z. Wen, X. Sun, Self-Powered Active Spherical Triboelectric Sensor for Fluid Velocity Detection, IEEE Transactions on Nanotechnology. 19 (2020) 230–235. https://doi.org/10.1109/TNANO.2020.2976154.

[47] C. Fan, C. Wu, G. Wen, A. Wang, Q. Zhou, Development of self-powered bubble velocity sensor for gas–liquid two-phase flow based on triboelectric nanogenerator, Nanotechnology. 32 (2020) 085503. https://doi.org/10.1088/1361-6528/abc7d7.

[48] Y. Wang, J. Wang, X. Xiao, S. Wang, P.T. Kien, J. Dong, J. Mi, X. Pan, H. Wang, M. Xu, Multi-functional wind barrier based on triboelectric nanogenerator for power generation, self-powered wind speed sensing and highly efficient windshield, Nano Energy. 73 (2020) 104736. https://doi.org/10.1016/j.nanoen.2020.104736.

[49] X. Wang, Y. Yang, Effective energy storage from a hybridized electromagnetic-triboelectric nanogenerator, Nano Energy. 32 (2017) 36–41. https://doi.org/10.1016/j.nanoen.2016.12.006.

[50] S. Wang, Z.L. Wang, Y. Yang, A One-Structure-Based Hybridized Nanogenerator for Scavenging Mechanical and Thermal Energies by Triboelectric–Piezoelectric–Pyroelectric Effects, Advanced Materials. 28 (2016) 2881–2887. https://doi.org/10.1002/adma.201505684.

[51] J. Chen, H. Guo, J. Zheng, Y. Huang, G. Liu, C. Hu, Z.L. Wang, Self-Powered Triboelectric Micro Liquid/Gas Flow Sensor for Microfluidics, ACS Nano. 10 (2016) 8104–8112. https://doi.org/10.1021/acsnano.6b04440.

[52] M. Wang, J. Zhang, Y. Tang, J. Li, B. Zhang, E. Liang, Y. Mao, X. Wang, Air-Flow-Driven Triboelectric Nanogenerators for Self-Powered Real-Time Respiratory Monitoring, ACS Nano. 12 (2018) 6156–6162. https://doi.org/10.1021/acsnano.8b02562.

[53] H. Guo, J. Chen, L. Tian, Q. Leng, Y. Xi, C. Hu, Airflow-Induced Triboelectric Nanogenerator as a Self-Powered Sensor for Detecting Humidity and Airflow Rate, ACS Appl. Mater. Interfaces. 6 (2014) 17184–17189. https://doi.org/10.1021/am504919w.

[54] Y. Su, G. Xie, F. Xie, T. Xie, Q. Zhang, H. Zhang, H. Du, X. Du, Y. Jiang, Segmented wind energy harvester based on contact-electrification and as a self-powered flow rate sensor, Chemical Physics Letters. 653 (2016) 96–100. https://doi.org/10.1016/j.cplett.2016.04.080.

[55] Y. Yang, G. Zhu, H. Zhang, J. Chen, X. Zhong, Z.-H. Lin, Y. Su, P. Bai, X. Wen, Z.L. Wang, Triboelectric Nanogenerator for Harvesting Wind Energy and as Self-Powered Wind Vector Sensor System, ACS Nano. 7 (2013) 9461–9468. https://doi.org/10.1021/nn4043157.

[56] H. Zou, Y. Zhang, L. Guo, P. Wang, X. He, G. Dai, H. Zheng, C. Chen, A.C. Wang, C. Xu, Z.L. Wang, Quantifying the triboelectric series, Nature Communications. 10 (2019) 1427. https://doi.org/10.1038/s41467-019-09461-x.

[57] Cylindrical Rotating Triboelectric Nanogenerator | ACS Nano, (n.d.). https://pubs.acs.org/doi/10.1021/nn402491y (accessed April 20, 2021).

[58] J. Wang, C. Wu, Y. Dai, Z. Zhao, A. Wang, T. Zhang, Z.L. Wang, Achieving ultrahigh triboelectric charge density for efficient energy harvesting, Nat Commun. 8 (2017). https://doi.org/10.1038/s41467-017-00131-4.

[59] 3M Scotch 33 Tape - Standard PVC Insulation Tape, Power and Cables. (n.d.). https://www.powerandcables.com/product/product-category/3m-scotch-33-tape/ (accessed April 21, 2021).

[60] J. Mihály, S. Sterkel, H.M. Ortner, L. Kocsis, L. Hajba, É. Furdyga, J. Mink, FTIR and FT-Raman Spectroscopic Study on Polymer Based High Pressure Digestion Vessels, Croatica Chemica Acta. 79 (2006) 497–501. https://hrcak.srce.hr/5664 (accessed April 18, 2021).

[61] M.R. Jung, F.D. Horgen, S.V. Orski, V. Rodriguez C., K.L. Beers, G.H. Balazs, T.T. Jones, T.M. Work, K.C. Brignac, S.-J. Royer, K.D. Hyrenbach, B.A. Jensen, J.M. Lynch, Validation of ATR FT-IR to identify polymers of plastic marine debris, including those ingested by marine organisms, Marine Pollution Bulletin. 127 (2018) 704–716. https://doi.org/10.1016/j.marpolbul.2017.12.061.

[62] A.R. Chowdhury, D. Lopez, A.M. Abdullah, M.J. Uddin, Polymer Based Cost-Effective Triboelectric Nanogenerator, in: AIChE, 2019. https://aiche.confex.com/aiche/2019/meetingapp.cgi/Paper/578431 (accessed January 31, 2020).

[63] E. Islam, A.M. Abdullah, A.R. Chowdhury, F. Tasnim, M. Martinez, C. Olivares, K. Lozano, M.J. Uddin, Electromagnetic-triboelectric-hybrid energy tile for biomechanical green energy harvesting, Nano Energy. 77 (2020) 105250. https://doi.org/10.1016/j.nanoen.2020.105250.

[64] A.M. Abdullah, A. Flores, A.R. Chowdhury, J. Li, Y. Mao, M.J. Uddin, Synthesis and fabrication of self-sustainable triboelectric energy case for powering smart electronic devices, Nano Energy. 73 (2020) 104774. https://doi.org/10.1016/j.nanoen.2020.104774.

[65] Make a Digital Voltmeter Using an Arduino - Projects, (n.d.). https://www.allaboutcircuits.com/projects/make-a-digital-voltmeter-using-the-arduino/ (accessed May 2, 2021).

[66] Interfacing Voltage Sensor with Arduino - Measure up to 25V using Arduino, Electronics Hub. (2018). https://www.electronicshub.org/interfacing-voltage-sensor-with-arduino/ (accessed May 2, 2021).

BIOGRAPHICAL SKETCH

Farzana Tasnim received her Master of Science degree in Chemistry in May 2021 of at the University of Texas Rio Grande Valley (UTRGV), Texas, United States. She completed her B.Sc. in Chemical Engineering and Polymer Science from Shahjalal University of Science and Technology, Bangladesh in 2013. She works in Photonics and Energy Research Laboratory (PERL) under Dr. M. Jasim Uddin's supervision. She was awarded the prestigious Presidential Graduate Research Assistantship from the Graduate College of UTRGV in 2019. Her research mainly focuses hybridization of nanogenerators using nanostructured functional interfaces, renewable energy, and electromechanical sensors. She can be reached at trisha.cep@gmail.com.